




# A one-stop strategy to search for long-duration gravitational-wave signals

Rodrigo Tenorio <sup>1,2,3,\*</sup>, Joan-René Mérou <sup>3</sup> and Alicia M. Sintès <sup>3</sup>

<sup>1</sup>*Dipartimento di Fisica “G. Occhialini”, Università degli Studi di Milano-Bicocca, Piazza della Scienza 3, 20126 Milano, Italy*

<sup>2</sup>*INFN, Sezione di Milano-Bicocca, Piazza della Scienza 3, 20126 Milano, Italy*

<sup>3</sup>*Departament de Física, Universitat de les Illes Balears, IAC3 – IEEC, Carretera Valldemossa km 7.5, E-07122 Palma, Spain*

Blind continuous gravitational-wave (CWs) searches are a significant computational challenge due to their long duration and weak amplitude of the involved signals. To cope with such problem, the community has developed a variety of data-analysis strategies which are usually tailored to specific CW searches; this prevents their applicability across the nowadays broad landscape of potential CW source. Also, their sensitivity is typically hard to model, and thus usually requires a significant computing investment. We present **fasttracks**, a massively-parallel engine to evaluate detection statistics for generic CW signals using GPU computing. We demonstrate a significant increase in computational efficiency by parallelizing the brute-force evaluation of detection statistics without using any computational approximations. Also, we introduce a simple and scalable post processing which allows us to formulate a generic semi-analytic sensitivity estimate algorithm. These proposals are tested in a minimal all-sky search in data from the third observing run of the LIGO-Virgo-KAGRA Collaboration. The strategies here discussed will become increasingly relevant in the coming years as long-duration signals become a standard observation of future ground-based and space-borne detectors.

## I. INTRODUCTION

Continuous gravitational waves (CWs) are long-duration gravitational-wave signals (GWs) [1]. For the current network of detectors operated by the LIGO-Virgo-KAGRA Collaboration (LVK) [2–4], the expected source of these signals are rapidly-rotating non-axisymmetric neutron stars in our Galaxy [5–7], although more exotic scenarios such as the evaporation of boson clouds around spinning black holes [8–12], dark matter halos [13–16], or sub-solar mass compact binaries [17–19] have been proposed as plausible sources, enriching the scientific scope of CW searches. Due to their extended duration, these signals are modulated by the motion of the detectors [20, 21], and span a parameter space at the edge of current computing capabilities [22, 23].

Future ground-based and space-borne detectors (Einstein Telescope [24], Cosmic Explorer [25], LISA [26], Taiji [27], TianQin [28]) will extend the operational bandwidth into lower frequencies of the GW spectrum. In such regime, GWs from compact binary coalescences (including those detected today using LVK data [29, 30]) are expected to be observable for a significantly longer time [31], bringing them qualitatively closer to CWs. This suggests current GW data-analysis algorithms will have to be revisited to make an efficient use of the available computing resources.

These past decades have seen a wide variety of developments to search for CWs from unknown sources (also known as *blind searches*) [20, 32–34]. Fundamentally, most of these approaches are distinguished by their specific sensitivity-cost trade-offs, which materialize in the form of different detection statistics, post-processing methods, and follow-up steps [35].

Although very successful, implementation details prevent their general applicability to more general phenomena, such as NS glitches [36, 37], spin wandering [38], proper motion [39], parallax effects [40], post-glitch [41] and post-merger [42, 43] CW-like signals, or different kinds of bosons [44]. Similar problems will be faced by compact-binary-coalescence analyses as we progress into next-generation detectors [45]. These science cases, which are relevant for both the first detection of a CW signal and future GW searches in general, require a general and efficient long-duration GW search pipeline in order to understand the current state of the art and inform future developments in GW data analysis.

We present **fasttracks**, a massively-parallel engine to compute short-coherence detection statistics for long-duration GW searches. **fasttracks** parallelizes the evaluation of detection statistics based on *time-frequency tracks* across multiple templates; in particular, it is capable of implementing any detection statistic based on Short Fourier Transforms (SFTs) [46–48]. Our results show that the use of GPU-accelerated brute-force template evaluation provides comparable computing efficiencies to using model-specific optimizations such as [33, 49–52]. We release **fasttracks** as an open-source Python package [53].

Building on **fasttracks** we propose a simple post-processing strategy to efficiently parallelize the identification of interesting candidates. With this, We generalize the semi-analytic sensitivity estimate algorithms introduced in [54, 55] to a broader class of detection statistic and to account for the effect of post-processing steps on the search. This method, which we released under the open-source **cows3** Python package [56, 57], will significantly reduce the computing cost associated to estimating the sensitivity of blind CW searches.

We test our proposals on a blind search for binary

\* [rodrigo.tenorio@unimib.it](mailto:rodrigo.tenorio@unimib.it)

CW sources using data from the LVK’s third observing run [58].

The paper is structured as follows: We review short-coherence detection statistics in Sec. II and present an efficient implementation using GPUs in Sec. III. In Sec. IV we discuss a simple template bank and post-processing strategy. These results are collected in Sec. V to propose a generalized semi-analytic sensitivity estimate method. We test the performance of our proposals on real data in Sec. VI. We conclude in Sec. VII.

## II. SHORT-COHERENCE CW SEARCHES

Blind CW searches use *semicoherent* methods in order to cover broad parameter-space regions under affordable computing budgets [33, 59, 60]. The overall idea of a semicoherent method is to divide data into segments that are analyzed independently to then construct a combined detection statistic. Different semicoherent methods are possible, depending on the chosen duration of the data segments and how different detectors are combined.

In this work we will treat the case of “short-coherence” CW searches, in which 1) different detectors are treated independently and 2) CW signals are monochromatic within the duration of a data segments. This denomination includes most of the current searches based on normalized-power or number-count statistics [33, 49–52, 61, 62]. The use of a short coherence time increases their robustness to unmodeled physics such as NS glitches or spin wandering [36, 38].

This section summarizes the main results in short-coherence detection statistics. The results here presented will be referred to later in the paper whenever new developments are presented.

### A. Signal model

We use the standard quasi-monochromatic CW signal model [34] parametrized by two sets of parameters: the amplitude parameters  $\mathcal{A}$  and the frequency-evolution parameters  $\lambda$ . The amplitude parameters include the CW amplitude  $h_0$ , the initial phase  $\phi_0$ , the (cosine of the) inclination angle  $\cos \iota$ , and the polarisation angle  $\psi$ . These two latter angles will be collectively referred to as  $\hat{\mathcal{A}} = \{\cos \iota, \psi\}$ . The frequency-evolution parameters  $\lambda$  depend on the signal of interest. Although the results in this work will be general, specific numerical results will be given for the case of a CW source in a circular binary system [52, 63, 64],

$$f(t; \lambda) = f_0 \left[ 1 + \frac{\vec{v}(t)}{c} \cdot \hat{n} - a_p \Omega \cos(\Omega t + \phi_b) \right] \quad (1)$$

i.e.  $\lambda = \{f_0, \hat{n}, a_p, \Omega, \phi_b\}$ , where  $f_0$  is the CW frequency at the start of the observation in the Solar System Barycenter,  $\hat{n}$  is the sky position of the source,  $a_p$  is the projected semimajor axis,  $\Omega$  is the binary orbital frequency, and  $\phi_b = -t_{\text{asc}}\Omega$  is an orbital phase where

$t_{\text{asc}}$  is the time of passage through the ascending node. Note that the source’s intrinsic frequency evolution is neglected; this is a reasonable assumption for short-coherence searches [52]. For convenience, individual components of  $\lambda$  will be indexed using square brackets  $\lambda[k]$ .

### B. Short-coherence detection statistics

We assume  $x$  consists of a series of Short Fourier Transforms [33, 46] with duration  $T_{\text{SFT}}$  labeled by an index  $\alpha$  and a detector-index  $X^1$ . The value of an SFT at timestamp  $t$  and frequency  $f$  will be denoted as  $\tilde{x}[t; f]$ . The total number of SFTs will be denoted as  $N_{\text{SFT}}$ .

The general form of a short-coherence detection statistic  $s$  is given by

$$s(\lambda) = \sum_{X, \alpha} w_{X\alpha}(\hat{\mathcal{A}}, \lambda) s[t_{X\alpha}; f(t_{X\alpha}; \lambda)]. \quad (2)$$

Here,  $w_{X\alpha}(\hat{\mathcal{A}}, \lambda)$  is an SFT-dependent weight encoding information about the noise floor, the detector’s sensitivity, and possibly the signal’s amplitude parameters. Whenever required we will use the weights introduced in [65], which are suitable for all-sky searches for isotropically-oriented sources [66]:

$$w_{X\alpha}(\hat{n}) \propto \frac{a^2(t_{X\alpha}; \hat{n}) + b^2(t_{X\alpha}; \hat{n})}{S_{nX\alpha}}. \quad (3)$$

$a$  and  $b$  are the detector’s response functions [20] and  $S_{nX\alpha}$  is the single-sided power spectral density of the noise. Weights are defined up to a constant which we are free to set so that

$$\sum_{X, \alpha} w_{X\alpha}(\hat{n}) = 1. \quad (4)$$

$s[t; f]$ , on the other hand, is a function of  $\tilde{x}[t; f]$  at the given timestamp  $t$  but possibly an arbitrary number of frequencies [67]. In this derivation we will focus on *normalized power*<sup>2</sup>

$$s[t; f] = \frac{4}{T_{\text{SFT}} S_n} |\tilde{x}[t; f]|^2. \quad (5)$$

The set of all  $s[t; f]$  values is commonly referred to as the *normalized spectrogram* of the data, an example of which we show in Fig. 1. Equation (2) could thus be intuitively described as the integration of power following a time-frequency “track” defined by a specific template  $\lambda$  across the spectrogram.

Additionally in Sec. VI we will make use of the *number count*, which is defined as [33]

$$\text{nc}[t; f] = \begin{cases} 1 & \text{if } s[t; f] > 3.2 \\ 0 & \text{otherwise} \end{cases}. \quad (6)$$

<sup>1</sup> Consecutive timestamps may differ by more than  $T_{\text{SFT}}$  if there are gaps in the data.

<sup>2</sup> Note that this corresponds to  $2\rho_k$  in [33].

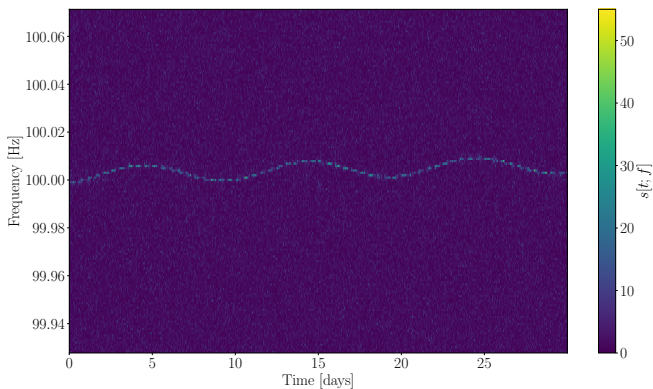


FIG. 1. Normalized spectrogram of 1 month of narrow-band simulated Gaussian noise as measured by the LIGO Hanford detector using  $T_{\text{SFT}} = 1024$  s. Data contains Gaussian noise with  $S_n = 10^{-23}$  and a binary CW signal with an amplitude of  $h_0 = 2 \times 10^{-24}$  visible as a high-power oscillating track at about 100 Hz. Amplitude modulations are due to the anisotropy of the detector, while frequency modulations are due to the binary orbital period of 10 days. Daily and yearly Doppler modulations are too small and too long, respectively, to be observed at these scales.

and can be used to define the *weighted number count* akin to Eq. (2). The threshold 3.2 corresponds to the optimal choice in Gaussian noise, in the sense discussed in [33]; other definitions are thoroughly used in the literature [49].

We now derive the distribution of  $s$  under both the noise and signal hypotheses.

### 1. Distribution under the noise hypothesis

Under the noise hypothesis, data is assumed to consist of white Gaussian noise with a given power-spectral density  $S_n$

$$\mathcal{H}_G : \tilde{x} = \tilde{n}, \quad (7)$$

where the real  $\Re$  and imaginary  $\Im$  parts follow the same distribution given by

$$\Re \tilde{n}[t; f], \Im \tilde{n}[t; f] \sim \text{Gauss} \left( 0, \frac{1}{2} \sqrt{T_{\text{SFT}} S_n} \right), \quad (8)$$

and the standard deviation follows from the Wiener-Kintchine theorem. Normalized power is then given by

$$\mathcal{H}_G : s[t; f] = \frac{4}{T_{\text{SFT}} S_n} |\tilde{n}[t; f]|^2. \quad (9)$$

Note that the variance of both  $\Re \tilde{n}$  and  $\Im \tilde{n}$  is equal and given by  $T_{\text{SFT}} S_n / 4$ . As a result,  $s[t; f]$  is the sum of two zero-mean unit-variance Gaussian variables and thus follows a chi-squared distribution with 2 degrees of freedom

$$s[t; f] | \mathcal{H}_G \sim \chi_2^2. \quad (10)$$

Normalized power  $s(\lambda)$  is thus the weighted sum of chi-squared distributed variables. This distribution does not have a simple closed form, but it can be efficiently simulated by generating  $N_{\text{SFT}}$  draws from a  $\chi_2^2$  distribution and computing the corresponding weighted sum. In the limit of  $N_{\text{SFT}} \gg 1$ , (typically  $N_{\text{SFT}} \sim \mathcal{O}(10^3\text{--}4)$ ), Lyapunov's Central Limit Theorem implies

$$s(\lambda) | \mathcal{H}_G \sim \text{Gauss}(\mu_G, \sigma_G) \quad (11)$$

where

$$\mu_G = 2 \sum_{X, \alpha} w_{X\alpha}, \quad (12)$$

$$\sigma_G^2 = 4 \sum_{X, \alpha} w_{X\alpha}^2. \quad (13)$$

Since weights  $w_{X\alpha}$  are defined up to a constant, we are free to choose a fixed value for  $\mu_G$  or  $\sigma_G^2$ .

Since we are operating in terms of SFTs, in a practical implementation the noise hypothesis is usually relaxed to assume Gaussian noise with a given PSD only *within* an SFT, so that  $S_n$  varies in timescales longer than  $T_{\text{SFT}}$  [33, 47]. Also, as noted in [68], this derivation makes the assumption that the PSD  $S_n$  is *known*, which is used implicitly in Eq. (10) as

$$x \sim \text{Gauss}(0, \sigma) \rightarrow x/\sigma \sim \text{Gauss}(0, 1). \quad (14)$$

In practice,  $S_n$  is *estimated* from the data. As a result, the estimated PSD becomes a random variable itself and Eq. (14) ceases to be applicable. This implies that, strictly speaking,  $s[t; f]$  should be described using *ratio distributions*, in a similar manner to [69–71]. Our specific implementation of PSD estimation follows that of [33], which uses a running-median estimate as implemented in `XLALNormalizeSFT` [72]; as discussed in [68] and corroborated by our numerical experiments, in such case the effect of estimating  $S_n$  can be described by introducing a small upwards bias in  $\mu_G$  and  $\sigma_G$ . For our case, the running median is computed using 101 frequency bins implies a bias of about 1.2% for  $\mu_G$ .

### 2. Distribution under the signal hypothesis

Under the signal hypothesis data consist of white Gaussian noise with a known PSD  $S_n$  and a CW signal  $h$  with parameters  $\lambda, \mathcal{A}$ :

$$\mathcal{H}_S : \tilde{x} = \tilde{n} + \tilde{h}. \quad (15)$$

As previously discussed, within an SFT  $X\alpha$  a CW signal can be described as a monochromatic signal with frequency  $f(t_{X\alpha}; \lambda)$  and amplitude given by [33]

$$\begin{aligned} & \left| \tilde{h}_{X\alpha} \right| \\ & \approx 0.7737 \frac{T_{\text{SFT}}}{2} h_0 \left| F_+(t_{X\alpha}; \hat{n}, \psi) \frac{1 + \cos^2 \iota}{2} + F_\times(t_{X\alpha}; \hat{n}, \psi) \cos \iota \right| \end{aligned} \quad (16)$$

where  $F_{+, \times}$  are the polarization-dependent antenna-pattern functions and the numerical  $\approx 0.7737$  factor is due to the fact that the CW's frequency in an SFT can be uniformly distributed around a Fourier bin [67].

The presence of a deterministic signal in a frequency bin shifts the noise's Gaussian distribution without altering its variance. Specifically (and respectively for the imaginary part)

$$\mathcal{H}_S : \Re \tilde{x}_{X\alpha} \sim \text{Gauss} \left( \Re \tilde{h}_{X\alpha}, \frac{1}{2} \sqrt{T_{\text{SFT}} S_n} \right). \quad (17)$$

This implies  $s[t, f]$  is no longer zero-mean, but instead

$$\rho_{X\alpha}^2 = \langle s[t_{X\alpha}; f(t_{X\alpha}; \lambda)] \rangle = \frac{4}{T_{\text{SFT}} S_n} \left| \tilde{h}(t_{X\alpha}; f(t_{X\alpha}; \lambda)) \right|^2. \quad (18)$$

As a result,  $s[t, f]$  follows a non-central chi-squared distribution with two degrees of freedom

$$\mathcal{H}_S : s_{X\alpha} \sim \chi_2^2(\rho_{X\alpha}^2). \quad (19)$$

Once more, the distribution of  $s(\lambda) | \mathcal{H}_S$  does not have a closed form but can be efficiently simulated by simulating the individual  $s_{X\alpha}$  values. In the  $N_{\text{SFT}} \gg 1$  limit Lyapunov's Central Limit Theorem implies

$$s(\lambda) | \mathcal{H}_S \sim \text{Gauss}(\mu_S, \sigma_S) \quad (20)$$

where

$$\mu_S = \mu_G + \sum_{X,\alpha} \rho_{X\alpha}^2 w_{X\alpha} = \mu_G + \rho_1^2 \quad (21)$$

$$\sigma_S^2 = \sigma_G^2 + \sum_{X,\alpha} \rho_{X\alpha}^2 w_{X\alpha}^2 = \sigma_G^2 + \rho_2^2. \quad (22)$$

In this derivation we implicitly assumed we had access to the signal's frequency-evolution parameters  $\lambda$ . In a search, however, we will cover the parameter space with a discrete set of templates, implying that the *closest* template to the signal,  $\lambda'$ , will recover a fraction of the fully-matched detection statistic. This fraction can be characterized by means of the mismatch [73–75]

$$m(\lambda'; \lambda) = \frac{s(\lambda) - s(\lambda')}{s(\lambda) - \mu_G}. \quad (23)$$

The effects of mismatch can be simply introduced by reducing the value of the non-centrality parameters  $\rho_{1,2}^2 \rightarrow (1 - m)\rho_{1,2}^2$ . The expected distribution of  $m$  depends on the chosen template bank. We will focus on the case of random template banks in Sec. IV.

Note that, for a given observing run, the distribution of  $s(\lambda)$  depends ultimately on four parameters  $\{\mu_G, \sigma_G, \rho_1^2, \rho_2^2\}$ . This will be exploited in Sec. V to efficiently estimate the sensitivity of a short-coherence CW search. It will also be convenient to define the amplitude-independent quantity

$$\hat{\rho}_{X\alpha}^2(\hat{\mathcal{A}}, \hat{n}) = \left( \frac{S_n}{h_0^2} \right) \rho_{X\alpha}^2(\hat{\mathcal{A}}, \hat{n}). \quad (24)$$

### III. ACCELERATING SHORT-COHERENCE DETECTION STATISTICS

The main stage of a blind CW search is to evaluate a detection statistic  $s$  on a template bank, which is a set of waveform templates  $\{\lambda_i, i = 1, \dots, N_T\}$  where each template  $\lambda_i$  contains the relevant parameters to describe a signal and usually  $N_T \sim \mathcal{O}(10^{12-18})$  [34]. Much of the CW literature is devoted to design smart search pipelines that exploit parameter-space correlations to make the computation of  $s$  more efficient, usually with a small cost in sensitivity [33, 49–52, 61, 62, 76–88].

Lately, several of these pipelines have been *re-implemented* using CUDA [89] (or similar low-level languages) to benefit from GPU acceleration [52, 90–92]. Specifically, these works re-implement a pre-existing computationally efficient strategy, such as *Partial Hough Maps* [33] or the  $\mathcal{F}$ -statistic's *Resampling* algorithm [78, 81, 93], and parallelize its evaluation on a GPU. This results in the *batch-evaluation* of waveform templates across limited portions of the parameter space (e.g. multiple sky positions [33] for a subset of frequency bins or multiple frequency bins for a fixed sky position [78, 81, 93]).

These approaches, while effective, were developed with a different computational landscape in mind, and may not be suitable (or required) given the computing capabilities of contemporary hardware. Also, as previously discussed, they may prevent their generalization to other astrophysically-plausible sources.

Here, we parallelize the brute-force evaluation of a short-coherence detection statistics without using pipeline-specific implementation tricks. We implement the computation of Eq. (2) in `fasttracks` [53] using `jax` [94, 95], which for our purposes can be thought as a GPU-capable implementation of Python's array library `numpy` [96]. Any other GPU-capable array library would be equally feasible for this implementation [97, 98]. The use of such high-level languages, which allow for a fast development cycle and simple code maintenance, is in stark contrast with other GPU-capable CW-searches [52, 90, 92].

A brute-force single-template evaluation of  $s(\lambda)$  uses the frequency-evolution track  $f(t; \lambda)$  to sum individual spectrogram bins  $s[t; f(t; \lambda)]$ . These operations are trivially implemented using array slicing and reduce operations. To evaluate multiple templates at once, we *vectorize*  $s(\lambda)$  using `jax`'s `vmap` function<sup>3</sup>. More precisely, we denote a *batch* of  $n$  templates by  $\vec{\lambda} = \{\lambda_1, \dots, \lambda_n\}$ . `vmap` promotes a single-template function  $s : \lambda \rightarrow s(\lambda)$  to a vectorized function `vmap`  $s : \vec{\lambda} \rightarrow \{s(\lambda_i), i = 1, \dots, n\}$  in such a way that the evaluation of different templates is parallelized on the available computing device. Note that we made *no assumption* on the properties of  $\vec{\lambda}$  (i.e.

<sup>3</sup> We could also vectorize by hand using other array frameworks [97, 98], but we choose to use `vmap` for its conceptual simplicity.



we are not restricted to fixed frequencies or fixed sky positions).

We benchmark the GPU-accelerated evaluation of `vmaps` [Eq. (2)] on an NVIDIA Hopper H100 GPU using a random template-bank of templates consistent with a CW source in a binary system. Templates are randomly sampled in frequency, sky position, and binary orbital parameters as discussed in Sec. IV. The resulting average cost per template is shown in Fig. 2.

Overall, the results are about two orders of magnitude faster than what we obtain using a CPU Intel Xeon Platinum 8460Y, and comparable to GPU implementations of *specific* search pipelines such as [52, 91] using similar statistics and number of SFTs. We thus conclude that `fasttracks` [53] provides a simple, efficient, and easily-generalizable implementation of short-coherence detection statistics.

We find that the average computing cost per template  $c_\lambda$  is described by the following model

$$\log_{10} c_\lambda = -\frac{5}{3} \log_{10} n + \frac{\log_{10} N_{\text{SFT}}}{1 + (10^6/n)^{5/6}} \quad (25)$$

This includes generating random templates, computing the corresponding frequency indices, gathering them, and then reducing the operation. The computational efficiency of `fasttracks` is primarily dominated by the number of templates evaluated in parallel. Upon saturating the capacity of the GPU, however, the cost becomes dominated by the number of  $N_{\text{SFT}}$ , which is proportional to the amount of numbers to add up to compute a statistic (i.e. the the average cost approaches the dotted line in Fig. 2). This was already noted in [86], where the main semicoherent computation is run over a smaller amount of coherent segments rather than over SFTs. Further computing gains are thus expected from the summation of less semicoherent segments.

These results show that *significant speed ups can be achieved solely due to the batch-evaluation of a high number of waveform templates on a GPU, regardless of whether a pipeline-specific optimization is being used.* This automatically generalizes the results discussed in [52, 90–92] to *any* sort of short-coherence search as long as a frequency-evolution model  $f(t; \lambda)$  is available.

#### IV. COMPRESSING WIDE PARAMETER-SPACE SEARCHES

As discussed in Sec. III, blind CW searches analyze a formidable amount of templates to cover the parameter space under consideration. Templates are usually deployed using lattices [23, 75, 99, 100] to benefit from computing optimizations [33, 49, 77, 82, 101]. Upon completion, the sensitivity of a search is generally dominated by the “loudest candidates” (i.e. templates with the maximum detection statistic) [102–105]. Search sensitivity can be increased by following-up an increasing number of candidates, especially if the parameter space is polluted by instrumental artifacts [56, 106]. This

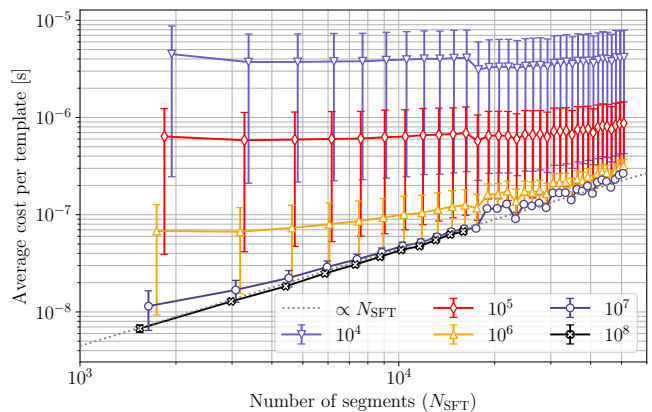


FIG. 2. Cost of evaluating `vmaps` on an NVIDIA Hopper H100 GPU. The vertical axis shows the average evaluation cost of a template, computed by evaluating a batch and dividing by the number of elements in the batch. The horizontal axis shows the number of SFTs in the dataset. Different markers represent different batch sizes. The dotted line is proportional to the number of SFTs and represents the point at which the computation becomes dominated by the summation of powers. Each measurement is the average across 10 different realizations. Points with the same  $N_{\text{SFT}}$  are nudged to avoid overlap of markers.

motivates the use of post-processing methods [107–112], to ascribe candidates to common causes. As a result, correlated candidates are analyzed together and the sensitivity increases, for a given number of selected candidates, compared analyzing individual candidates.

The computational gains demonstrated in Sec. III grant us the freedom to rethink the template-bank (Sec. IV A) and post-processing (Sec. IV B) setups to accommodate our needs. We aim to formulate a simple, easy-to-model signal-agnostic setup that fully exploits the capabilities of `fasttracks`. We will make use of these developments in Sec. V to provide a generic sensitivity-estimate method and in Sec. VI to deploy a search in real data.

##### A. Template bank setup

Two main ingredients are required to set a template bank up, namely a notion of “closeness” amongst templates and a template-placement prescription. These have been thoroughly studied for long-coherence statistics [22, 23, 32, 63, 64, 77, 82, 100, 101, 113, 114], but not so much for short-coherent searches (with the notable exception of [86]). We here propose a simple approach to construct template banks for short-coherence detection statistics. While our specific application will be a blind search for CW sources in binary systems, the general principles here described should be applicable to most kinds of CW searches.

### 1. A notion of “closeness”

Short-coherence detection statistics [Eq. (2)] depend on  $\lambda$  mainly through the frequency-evolution model  $f(t; \lambda)$ , from which a parameter-space distance can be defined [109]. For a given spectrogram time-resolution  $T_{\text{SFT}}$ , frequency is naturally discretised in steps of  $T_{\text{SFT}}^{-1}$ . We can thus define the parameter-space resolution of a given parameter  $\delta\lambda[k]$  as the minimal variation so that the resulting frequency track differs by about one frequency bin along the frequency evolution:

$$\delta\lambda[k] = \frac{1}{T_{\text{SFT}}} \left| \frac{\partial}{\partial\lambda[k]} f(t; \lambda) \right|^{-1}. \quad (26)$$

This prescription, which is standard for short-coherence detection statistics [33, 49–51], may yield time-dependent parameter-space resolutions, in which case we will conservatively take the minimum value of  $\delta\lambda[k]$ . As shown in App. A, Eq. (26) yields the expected functional dependency of  $\delta\lambda$  on  $\lambda$  for the case of short-segment semicoherent detection statistics [33, 63, 64]. The number of required templates to cover a parameter space region  $\Delta\lambda$  is then given by

$$\mathcal{N}(\Delta\lambda) = \int_{\Delta\lambda} d\lambda \prod_{k=1}^D \frac{1}{\delta\lambda[k]}. \quad (27)$$

where  $D$  is the number of dimensions that can be resolved. This expression “counts” the number of subdivisions of “size”  $\delta\lambda$  required to cover  $\Delta\lambda$  for a non-constant  $\delta\lambda$ . Note that this prescription does not take into account parameter-space correlations of the detection statistic (cf. [23, 63, 64, 73, 114, 115].)

The relative importance of different parameter-space regions can be quantified by the “local template density”

$$\varrho(\lambda) = \prod_{k=1}^D \frac{1}{\delta\lambda[k]} \quad (28)$$

which can be used to guide template-placement algorithms. This quantity plays a similar role to the *volume element* derived from the determinant of the parameter-space metric [63, 64, 73, 74, 77, 113]. In such setups, the parameter-space metric, which is related to Eq. (23), can be used to guarantee a parameter-space coverage with a maximum mismatch [113, 114]. Here, on the other hand,  $\varrho(\lambda)$  quantifies deviations in the frequency evolution. This is enough to distinguish templates, but requires the use of numerical methods to understand the mismatch distribution and thus the sensitivity impact on a search, as we will discuss shortly.

Several methods are available to construct a template bank with a non-constant density  $\varrho(\lambda)$  [63, 74, 113, 116]. We here propose a simple strategy. For usual all-sky searches (see App. A for a worked example) [33, 52],  $\varrho(\lambda)$  is a monomial in  $\lambda$

$$\varrho(\lambda) = C \prod_{k=1}^D \lambda[k]^{p_k}, \quad (29)$$

where the  $p_k$  exponents depend on the specific CW model and  $C$  is an overall constant. As a result, we can define a new set of coordinates  $\xi(\lambda)$  so that  $\varrho(\xi) = 1$ :

$$d\lambda \varrho(\lambda) = d\xi. \quad (30)$$

By means of Eq. (29), we can split Eq. (30) into component-wise equations

$$\frac{d\xi[k]}{d\lambda[k]} = \sqrt[p_k]{C} \lambda[k]^{p_k}, \quad (31)$$

which implies

$$\xi[k] = \frac{\sqrt[p_k]{C}}{p_k + 1} \lambda[k]^{p_k + 1}. \quad (32)$$

This defines a bijection between the physical parametrization  $\lambda$  and the *uniform-density* parametrization  $\xi$  whose inversion is trivial. Sampling *uniformly* on the  $\xi$  space corresponds to sampling according to  $\varrho(\lambda)$  in  $\lambda$ .

The generation of a template bank for a non-uniform density  $\varrho(\lambda)$  such as that described in Eq. (29) goes then as follows: For a given parameter space region  $\Delta\lambda$ ,

1. Map the boundaries in  $\Delta\lambda$  to the boundaries in  $\xi$  using Eq. (32):

$$\begin{aligned} \xi_{\min} &= \xi(\lambda_{\min}) \\ \xi_{\max} &= \xi(\lambda_{\max}) \end{aligned}$$

2. Generate a template bank in  $\xi$  according to any prescription.
3. Map the template bank in  $\xi$  back to  $\lambda$  using Eq. (32).

### 2. Random template bank

$\xi$  coordinates allow for standard lattice template-bank construction methods [74, 113]. Here, on the other hand, we explore the use of *random* template banks [115, 117]. These are easy to implement in our setup and play nicely with the batch-evaluation of templates: Instead of walking a grid, simply draw  $n$  templates uniformly in  $\xi$ , map them to  $\lambda$ , and evaluate the detection statistic using `vmap s`. The expected sensitivity loss of a random template bank compared to that of an optimal quantize tends to decrease with the parameter-space dimensionality [75]. This makes them well suited for our work, as we will be ultimately interested in the problem of unknown CW sources in binary systems ( $D \geq 6$ ).

We characterize random template banks in this setup by means of the *oversampling*  $o$ , which corresponds to the ratio of templates in the template bank over the number of templates in the covered region according to Eq. (27).

For a given parameter-space region  $\Delta\lambda$ , the mismatch distribution  $p(m|o)$  can be sampled as follows:

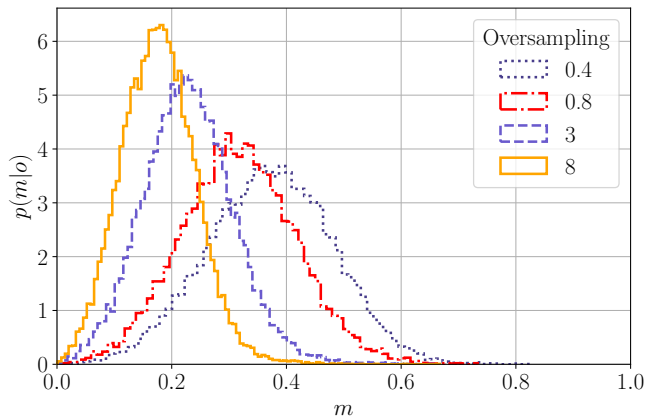


FIG. 3. Mismatch distributions for the search setup described in Sec. VI using Gaussian noise. The results shown here correspond to a frequency of about 100 Hz; comparable results are obtained for other frequency bands.

1. Generate a Gaussian-noise data stream containing a CW signal according to the search’s priors.
2. Uniformly sample  $o\mathcal{N}(\Delta\lambda)$  templates in  $\xi$  space and map them to  $\lambda$  space.
3. Evaluate `vmaps` on the generated templates and compute  $m$  according to Eq. (23).

We show the mismatch distribution corresponding to the search setup described in Sec. VI for different oversampling values in Fig. 3. Concretely, templates are uniformly distributed in a narrow frequency band of 0.125 Hz, across the sky, and across the binary parameter-space region described in Sec. VI. We use simulated Gaussian noise in a consistent manner with the dataset described in Sec. VI. These results correspond to a frequency of about 100 Hz; different frequency bands yield similar results, as expected from the definition of  $\xi$ . As we shall discuss in Sec. V, these distributions allow us to connect computing-cost related quantities (such as oversampling  $o$ ) to sensitivity-related quantities (such as mismatch  $m$ ). The results seem to be compatible with Weibull distributions for average mismatch values away from  $m = 0$  and  $m = 1$ . This is compatible with the expected result from extreme value theory [103]. For increasing values of  $o$ , the mismatch reduction slows down with respect to  $o$ , as discussed in [115].

### B. Ahead-of-time clustering

As previously discussed, post-processing strategies [107–112] work by grouping together nearby candidates in the parameter space, usually by means of a clustering algorithm. This has the effect of reducing the detectability threshold at a given follow-up cost [56]. Ultimately, however, the operative result of these algorithms is to select *uncorrelated local maxima* across

the parameter space. One could propose a simpler post-processing approach by splitting the parameter-space into disjoint regions so that the search step consists in retrieving the loudest candidate within each region.

Meaningfully dividing the parameter space is in general difficult due to the dependency of the parameter-space metric with the parameter-space position itself. We here propose a simpler approach using the  $\xi$  coordinates to divide region  $\Delta\lambda$  into disjoint hyperboxes with a constant number of templates. To do so, note that, by construction,

$$\mathcal{N}(\Delta\lambda) = \prod_{k=1}^D \Delta\xi[k], \quad (33)$$

i.e. the number of templates in a region  $\Delta\lambda$  is the *coordinate volume* enclosed in  $\xi$ . Boxes with a fixed number of templates, say  $n_b$ , can be created by partitioning  $\Delta\xi$  into regular hyperboxes with a coordinate volume of  $n_b$  templates. This approach is significantly simpler than a clustering, and could behave in a similar manner if hyperboxes are properly selected.

Statistically speaking, different boxes will have a different set of weights  $w_{X\alpha}(\lambda)$  as they will contain different templates  $\lambda$ . Since we work in the  $N_{\text{SFT}} \gg 1$  limit, in which  $s$  follows a Gaussian distribution, it is enough to standardise the detection statistic to a zero-mean unit-variance Gaussian distribution to make comparisons across different boxes

$$z(\lambda; b) = \frac{s(\lambda) - \mu_G(b)}{\sigma_G(b)}. \quad (34)$$

At this point, is up to the search setup to decide how many boxes to select. Note that *any* selection scheme is allowed, including deliberately rejecting boxes containing instrumental artifacts. The effect of rejecting a certain number of boxes can be negligible, if the number of boxes is high enough, as sensitivity estimates ultimately operate at 90% to 95% detection probability [35]. To decide the number of partitions, we ensure a minimum of 10,000 boxes in any narrow search frequency band (typically covering about 0.1 Hz) to allow for the rejection of highly contaminated regions, and cap the box size in such a way that the number of templates results in an efficient evaluation given the available GPUs at hand.

This ahead-of-time partition provides a unified picture of the post-processing algorithms used in short-coherent blind CW searches, as well as a simple and computationally efficient proposal of post-processing, as the memory, computing cost, and tuning parameters have been significantly reduced compare to previous approaches.

### V. SENSITIVITY OF A SHORT-COHERENCE SEARCH

The sensitivity of a blind CW search is typically expressed in terms of the minimal amplitude  $h_0$  so

that a fraction  $p_{\text{det}}$  of an isotropically-oriented all-sky population of sources is detected [34, 35]. Typically, instead of  $h_0$  the results are stated in terms of the *sensitivity depth* [55, 118]

$$\mathcal{D} = \frac{\sqrt{S_n}}{h_0}, \quad (35)$$

which ends up a function of the search setup (the available dataset, the template-bank setup, and the detection statistic on use) and the signal population under consideration.

In an actual search, the estimation of  $\mathcal{D}$  is done numerically through the use of software-simulated signals (injections), which has an associated computing cost. This motivated the development of semi-analytic sensitivity estimate methods [54–56], which as implemented in [57, 119] have a negligible cost and can be used as a first step to guide in-depth injection campaigns. These methods, however, are developed specifically for the  $\mathcal{F}$ -statistic (or the associated number count [55]) and do not consider neither the case of weighted statistics nor the effect of post-processing steps.

Sensitivity estimates are ultimately rooted in the principles discussed in [120]: Given a search setup and signal distribution configuration  $c$ , the detection probability corresponds to the fraction of datasets  $x$  in the data space that satisfy a certain detection rule  $R(x; c)$ :

$$p_{\text{det}}(c) = \int dx R(x; c) p(x|c). \quad (36)$$

$p(x|c)$  represents a data generating process according to the specifications in  $c$ , such as a CW signal in Gaussian noise. If we fix a search setup and signal distribution, the dependency in  $x$  of Eq. (36) can be recast in terms of the detection statistic  $z$  and the parameter-space region at hand as

$$p_{\text{det}}(\mathcal{D}, o, \{\tau\}) = \int d\lambda \int dz R(z; \tau(\lambda)) p(z|\mathcal{D}, o, \lambda) p(\lambda), \quad (37)$$

where now the configuration  $c$  is given by the sensitivity depth of the population  $\mathcal{D}$ , the oversampling of the template bank  $o$  (see Sec. IV A), and the set of detectability thresholds  $\{\tau\}$ , which may depend on the parameter-space location as per Sec. IV B. We discuss the definition of  $p(z|\mathcal{D}, o, \lambda)$  in Sec. V A.

With this, estimating the sensitivity of a search, represented by the sensitivity depth  $\mathcal{D}^p$  at which a fraction  $p$  of the population is detected becomes solving the one-dimensional equation

$$p_{\text{det}}(\mathcal{D}^p, o, \{\tau\}) = p. \quad (38)$$

In practice,  $p_{\text{det}}$  is computed through Monte Carlo

integration

$$p_{\text{det}}(\mathcal{D}, o, \{\tau\}) \approx \frac{1}{N_I} \sum_{i=1}^{N_I} R(z^{(i)}; \tau(\lambda^{(i)})) \quad (39)$$

$$z^{(i)} \sim p(z|\mathcal{D}, o, \lambda^{(i)})$$

$$\lambda^{(i)} \sim p(\lambda)$$

This calculations amount to computing what fraction of  $N_I$  software-simulated signals is detected by the search pipeline. The process of simulating and running the search pipeline (i.e. computing the detection statistic) corresponds in Eq. (39) to sampling  $z^{(i)}$ , whereas deciding whether said signal is detected corresponds to evaluating  $R(z^{(i)}; \tau(\lambda^{(i)}))$ .

The basis for the semi-analytical sensitivity estimation algorithm proposed in [54, 55] is to derive an efficient formulation of  $p(z|\mathcal{D}, o, \lambda)$  so that it can be efficiently sampled. We generalize such an approach to short-coherence detection statistics in Sec. V A and the corresponding implementation of the detection rule  $R(z; \tau(\lambda))$  in Sec. V B. The method is summarized in Sec. V C.

## A. Simulating detection statistics

We now discuss a simple procedure to draw samples from  $p(z|\mathcal{D}, o, \lambda)$ , for which we need to results. First, note that given parameter-space partition around a template  $\lambda$  with known  $\mu_G$  and  $\sigma_G$ , sampling  $p(z|\mathcal{D}, o, \lambda)$  is equivalent to sampling  $p(s|\mathcal{D}, o, \lambda)$  and then computing  $z = (s - \mu_G)/\sigma_G$ . As a result we work in terms of  $s(\lambda)$  to directly apply the results derived in Sec. II. Second, we recall that we can introduce any hypothesis into a probability as long as we marginalize over it [121], i.e.

$$p(a|b) = \int d\phi p(a, \phi|b) = \int d\phi p(a|\phi, b) p(\phi|b) \quad (40)$$

where  $a$ ,  $b$ , and  $\phi$  are arbitrary parameters. Moreover, if  $\phi$  was sufficient to determine the distribution of  $a$  regardless of  $b$ , we could further simplify  $p(a|\phi, b)$  to  $p(a|\phi)$ .

We start by introducing explicit dependencies on the mismatch and the orientation angles in  $p(s|\mathcal{D}, o, \lambda)$ . The reason is that  $s$  can be sampled using Eq. (20) as long as we fix a specific parameter-space region and we know the depth  $\mathcal{D}$ , mismatch  $m$  and pair orientation angles  $\hat{\mathcal{A}}$ . To do so, we use Eq. (40) to marginalize over the mismatch  $m$  and orientation angles  $\hat{\mathcal{A}}$ :

$$p(s|\mathcal{D}, o, \lambda) = \int d\hat{\mathcal{A}} \int dm p(s|\mathcal{D}, m, \lambda, \hat{\mathcal{A}}) p(\hat{\mathcal{A}}) p(m|o), \quad (41)$$

$p(m|o)$  can be obtained numerically at a negligible cost as discussed in Sec. IV A. The distribution  $p(s|\mathcal{D}, m, \lambda, \hat{\mathcal{A}})$  corresponds to Eq. (20). We now proceed in a similar manner to [54, 55] and recognize that Eq. (20) depends on  $\hat{\mathcal{A}}$ ,  $\lambda$ , and the observing run configuration through



only 4 parameters  $q = \{\mu_G, \sigma_G, \hat{\rho}_1^2, \hat{\rho}_2^2\}$ . As a result, we can apply a similar argument once more to obtain

$$p(s|\mathcal{D}, o, \lambda) = \int dm \int dq p(s|\mathcal{D}, m, q) p(q|\lambda) p(m|o), \quad (42)$$

where the dependency on  $\lambda$  is contained within the weights  $w_{X\alpha}$  inside  $q$ .

The four quantities in  $q$  play an analogous role to the ‘‘response function’’ and similar quantities governing the distribution of the  $\mathcal{F}$ -statistic [54–56]. These four quantities are due to 1) the Gaussian distribution of  $s$  in the limit  $N_{\text{SFT}} \gg 1$ , which requires only *two* parameters to be characterized, and 2) the use of weights, which modify the distribution parameters under *both* the signal and noise hypotheses. Similar approaches are applicable for the treatment of other weighted statistics such as [86, 122].

Specifically,  $q$  is a set of deterministic function of the orientation parameters  $\hat{\mathcal{A}}$  and the sky position  $\hat{n}$ . Given a specific signal population, which fixes  $p(\hat{\mathcal{A}}, \hat{n})$ , we can numerically generate the distribution of  $q$  *once for a given observing run* as follows: First, we draw a set of sky position and amplitude parameters from the population priors

$$\hat{\mathcal{A}}^{(i)}, \hat{n}^{(i)} \sim p(\hat{\mathcal{A}}, \hat{n}). \quad (43)$$

These are combined with the SFT timestamps and antenna-pattern functions to compute the per-SFT data-dependent quantities

$$\begin{aligned} \hat{\rho}_{X\alpha}^2 &= \hat{\rho}_{X\alpha}^2(\hat{\mathcal{A}}^{(i)}, \hat{n}^{(i)}) \\ w_{X\alpha}^{(i)} &= w_{X\alpha}(\hat{n}^{(i)}) \end{aligned}, \quad (44)$$

which completely determine the four quantities in  $q$ :

$$\begin{aligned} \mu_G^{(i)} &= (1.012) \times 2 \sum_{X,\alpha} w_{X\alpha}^{(i)} \\ \sigma_G^2 &= 4 \sum_{X,\alpha} (w_{X\alpha}^{(i)})^2 \\ \hat{\rho}_1^2 &= \sum_{X,\alpha} w_{X\alpha}^{(i)} \hat{\rho}_{X\alpha}^2 \\ \hat{\rho}_2^2 &= \sum_{X,\alpha} (w_{X\alpha}^{(i)})^2 \hat{\rho}_{X\alpha}^2 \end{aligned}. \quad (45)$$

where the extra 1.012 factor in  $\mu_G^{(i)}$  corresponds to the PSD-estimation bias, as discussed in Sec. II.

## B. Detection rules

The second required ingredient is the detection rule, which is a function which decides whether a data realization contains a signal or not. In a CW search, this function encapsulates the effect of post-processing steps and other significance vetoes imposed in the resulting parameters. As a result, it is typically difficult to model

and most sensitivity estimation algorithms approximate it as a step function depending on the detectability threshold.

The specific post-processing proposed in Sec. IV B, however, allows for a simple modeling: The threshold against which a candidate is compared is a function of the parameter-space box in which said template falls. This corresponds to defining a function  $\tau(\lambda)$  which returns the corresponding detectability threshold, be it in terms of  $s$  or  $z$ . As a result, a general detection rule accounting for the effects our post-processing can be readily formulated as

$$R(z; \tau(\lambda)) = \begin{cases} 1 & \text{if } z > \tau(\lambda) \\ 0 & \text{otherwise} \end{cases}. \quad (46)$$

## C. Summary

Equation (38) can be easily solved by numerically computing  $p_{\text{det}}$  using a Monte Carlo integral as follows:

$$\begin{aligned} p_{\text{det}}(\mathcal{D}, o, \{t\}) &\approx \frac{1}{N_I} \sum_{i=1}^{N_I} \begin{cases} 1 & \text{if } z^{(i)} > \tau(\lambda^{(i)}) \\ 0 & \text{otherwise} \end{cases} \\ z^{(i)} &= [s^{(i)} - \mu_G(\lambda^{(i)})] / \sigma_G(\lambda^{(i)}) \\ s^{(i)} &\sim p(s|\mathcal{D}, m^{(i)}, q^{(i)}) \\ q^{(i)} &\sim p(q|\lambda^{(i)}) \\ \lambda^{(i)} &\sim p(\lambda) \\ m^{(i)} &\sim p(m|o) \end{aligned}. \quad (47)$$

The distributions associated to  $q$  and  $m$  are independent of  $\mathcal{D}$  and well-determined for a given search setup and sky-distribution. As a result, the evaluation of  $p_{\text{det}}(\mathcal{D}, o, \{t\})$  can be efficiently computed using any array-capable computing software. We release an implementation of  $p_{\text{det}}$  under the `cows3` package [56, 57].

Let us summarize the main result of this section: Sampling  $p(z|\mathcal{D}, o, \lambda)$  is statistically equivalent to injecting a CW signal in Gaussian noise at depth  $\mathcal{D}$  with orientation and sky location parameters drawn from  $p(\hat{\mathcal{A}}, \hat{n})$  and retrieving the maximum detection statistic  $z$  from a random template bank with oversampling  $o$ . The computing gains come from the fact that, once the distribution of  $q$  is computed, sampling  $p(z|\mathcal{D}, o, \lambda)$  is several orders of magnitude faster than generating software-simulated signals.

Note that, for this procedure to be applicable,  $p(z|\mathcal{D}, o, \lambda)$  only needs to be *sampled*, in a similar manner to the ‘‘synthetization’’ approach [41, 74, 122]. As a result, this approach is applicable to a broad array of detection statistics [41, 74, 122–125].

## VI. APPLICATIONS TO REAL DATA

We test the effectiveness of these developments on data from the first half of the LVK’s third observing run [58].

We deploy an all-sky search for unknown CW sources in binary systems in a selection of frequency bands, a setup similar to [126]: We select 8 representative 0.125 Hz frequency bands ([110.500, 132.625, 168.000, 187.000, 207.125, 228.625, 252.625, 260.625] Hz) where we deploy an all-sky search covering orbital periods of 7 to 15 days and projected semi-major axes of 5 to 15 light-seconds. We use SFTs with a duration of  $T_{\text{SFT}} = 1024\text{s}$  with a 50% overlap and windowed by a Tukey widow with a 0.5 tapering parameter [32]. The results will be presented in terms of population-based sensitivity estimates, which will be compared to the sensitivity estimates produced by the method in Sec. V.

### A. Search setup

The aim of this study is to showcase the applicability of the simple approaches presented throughout this work. To do so, we deploy an all-sky search in real data and compute the corresponding sensitivity estimates using different search setups. We assume that all the selected outliers would be followed-up and discarded by a more sensitive method such as [37, 56, 127, 128]. The results will be informative in that they would be equivalent to those obtained by an actual search if no signal is detected.

For each frequency, we deploy a template bank with using an oversampling of  $o = 3.44$ . This corresponds to about 1 million GPU computing hours to cover the full frequency band from 100 Hz to 300 Hz. We divide the parameter space in each band into hyperboxes containing about  $10^8$  templates, ensuring always a minimum of 10,000 boxes per band. To account for non-Gaussianities in the data, we compute detection statistics templates as discussed in Sec. VIB and retrieve the loudest template per box.

Upon completion of the main search stage we are left with a list of templates and their corresponding detection statistic  $\mathcal{T} = \{(\lambda_b, s_b), b = 1, \dots, N_{\text{boxes}}\}$ . In line with standard practice [56, 127, 128], a certain number of candidates  $N_{\text{cand}}$  is selected to follow-up. This procedure sets the corresponding detectability thresholds for the sensitivity estimate procedure. We test here two different post-processing approaches which intend to be comparable to those used in current post-processing algorithms [35].

The first approach is to select the top  $N_{\text{cand}}$  candidates in  $\mathcal{T}$ . This implies the detectability of a signal depends on the hyperbox where it falls: If the signal falls within a hyperbox containing a selected candidate, said signal is detected if it has a detection statistic above that of the candidate; otherwise, a signal is detected if it has a greater detection statistic than the last selected candidate.

A second approach makes use of the sensitivity procedure in Sec. V. Having access to  $\mathcal{T}$  implies we can numerically evaluate  $\mathcal{D}^{95\%}$  as a function of  $N_{\text{cand}}$  very efficiently. As a result, we can compute the outlier-selection strategy that *maximizes*  $\mathcal{D}^{95\%}$  for a given  $\mathcal{T}$ .

To do so, we sort the candidates in  $\mathcal{T}$  in descending order according to their detection statistic. We then allow  $N_{\text{reject}}$  hyperboxes to be *rejected* and  $N_{\text{cand}}$  hyperboxes to be selected. This allows for highly-disturbed regions containing noise artifacts to be ignored so that computing resources are better employed, in a similar manner to what was argued in [56]. The resulting detection rule is similar to that of the previous approach, except that signals in an ignored hyperbox are not detected. Note that this may give rise to diminishing returns, as rejecting too many boxes may end up hindering the search’s sensitivity.

We make use of this last approach, using the sensitivity estimate strategy developed in Sec. V to optimize the number of rejected and selected boxes. This procedure is computationally very efficient, as it only involves evaluating a handful of Monte Carlo integrals, and amounts to less than 1 minute on a laptop for a given frequency band.

The actual sensitivity of these different setups is then evaluated by means of an injection campaign. We inject 500 simulated signals at different, discrete depth values. These injections are isotropically oriented and uniformly distributed in the sky and the binary parameters [126]. From these, we compute the detected fraction of the population at a given depth.

### B. Particularities of real-data searches

Noise in a real-data search is generally non-Gaussian and contains different kinds of instrumental artifacts that degrade the sensitivity of a search [106]. This generally causes the results derived in Sec. V to be unapplicable, as the underlying distributions of  $s$  are practically unknown. One approach to overcome the effect of instrumental artifacts in CW searches is to design better suited detection statistics, such as [123, 124]. Here, we follow a simpler approach proposed in [129] using multiple detection statistics.

Non-Gaussianities are capable of accumulating a large amount of normalized power in a relatively “short” period of time <sup>4</sup>. As a result, the loudest template in a box can either be caused by a genuine CW signal or by a non-Gaussianity. The key property to tell these two phenomena apart relies on quantifying their *persistence*. This was initially discussed in [33] which proposed the use of the *number count* statistic. The weighted number count of a signal is compute using the binarized spectrogram according to some threshold, and provides an adequate notion of persistence.

We proceed in a similar manner to the approach proposed in [129]: We retrieve the candidate with the *loudest* normalized power with the extra restriction of

---

<sup>4</sup> Note that non-Gaussianities do not need to be short themselves; rather, it is enough that the frequency-evolution track of a signal overlaps such non-Gaussianity for a short period of time.

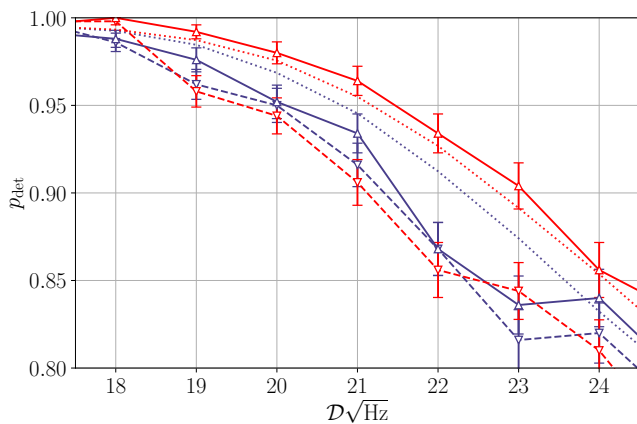


FIG. 4. Detection probabilities at different sensitivity depths for the signal population discussed in the text at 110.5 Hz. Each line corresponds to a different detection statistic and post-processing configuration. The blue lines correspond to retrieving the template with maximum normalized power without a minimal weighted number count; the red lines impose a minimal weighted number count as discussed in the text. The dashed lines correspond to  $N_{\text{cand}} = 1$ . The solid lines correspond to the optimal choice of  $N_{\text{reject}}$  and  $N_{\text{cand}}$ . The dotted lines show the estimated sensitivity for said optimal choice using the method from Sec. V

scoring *at least* a pre-established weighted number count value. We choose said value to be three standard deviations above the average number count in Gaussian noise, based on our numerical results. Statistics of the weighted number count are derived in [130].

### C. Results

We start by comparing these different approaches for the 110.5 Hz frequency band in Fig. 4. While for a low number of selected candidates  $N_{\text{cand}} = 1$  both approaches behave similarly, the use of a number-count filter significantly improves the detection probability towards higher depths (i.e. lower signal amplitudes) for the optimal candidate selection setup compared to only using normalized power. Furthermore, if a minimal number count is imposed, the measured detection probability is in agreement with the estimate provided by the method in Sec. V. This supports the idea that requiring a minimal persistency tames the effect of non-Gaussianities of the data.

After identifying the use of number count as a favorable choice, we show in Fig. 5 the effect of rejecting a certain number of boxes. Specifically, we compare the detection probabilities for  $N_{\text{cand}} = 1, 10, 100, 1000$  without rejecting boxes and using the optimal number of rejected boxes for each number of candidates. We observe that, for this specific case, the sensitivity depends weakly on  $N_{\text{cand}}$  once the optimal number of boxes has been rejected. This is consistent with the results of [56]: Loud candidates are caused by a

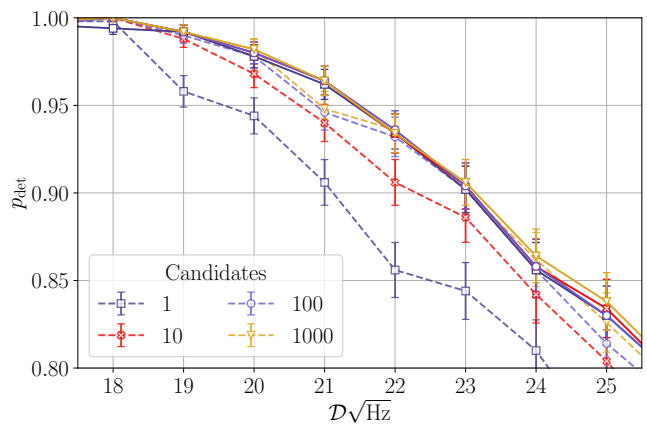


FIG. 5. Comparison of detection probabilities for different number of selected candidates  $N_{\text{cand}}$  imposing a minimal number count at 110.5 Hz. Dashed lines correspond to  $N_{\text{reject}} = 0$ , while solid lines use the optimal number of rejected boxes.

mixture of non-Gaussianities in the data and a Gaussian background. Non-Gaussianities tend to cause highly-correlated elevated normalized power structures that are well contained within a certain number of hyperboxes; extreme events caused by a Gaussian background, on the other hand, are scattered across the parameter space and scale weakly with the number of selected candidates [103]. As a result, the majority of the sensitivity gain is achieved upon rejecting all hyperboxes containing non Gaussianities.

We produce similar results for seven other frequency bands and compute the sensitivity depth at which 95% of the signals are detected. To do so, we fit a sigmoid to the detection probability and compute the corresponding uncertainty through the covariance matrix of the fit, as discussed in [126]. The results are shown in Fig. 6. We observe compatible results with those displayed by the 110.5 Hz band: Upon selecting an optimal number of rejected boxes, the resulting sensitivity is weakly dependent on number of candidates to follow-up. The specific gain depends on the properties of the background noise, which tends to behave differently depending on the frequency band.

The sensitivity depths here obtained are broadly consistent with those reported in [126]. This is expected, as both setups use the same detection statistics and  $T_{\text{SFT}}$ . In light of this result, we can conclude that the developments presented in this work are a feasible proposal to conduct broad parameter-space searches in future observing runs.

## VII. CONCLUSION

The search for CW signals from unknown sources is a formidable computational challenge due to the involved parameter-space breadths. To tackle such a problem, multiple detection pipelines benefiting from different

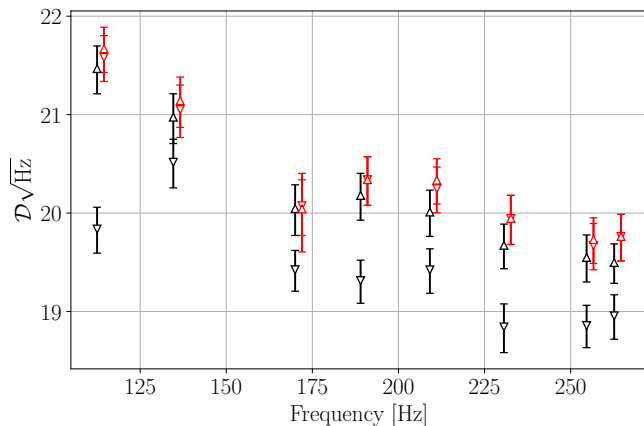


FIG. 6. Sensitivity depth corresponding to a 95% detection probability for eight representative frequency bands. All results are computed imposing a minimum number count as discussed in the main text. Downwards-pointing triangles correspond to  $N_{\text{cand}} = 1$ , while upwards-pointing triangles correspond to  $N_{\text{cand}} = 1000$ . Black markers correspond to  $N_{\text{reject}} = 0$ , while red markers correspond to choosing the optimal  $N_{\text{reject}}$  for the chosen number of candidates. Points with the same frequency are nudged to avoid overlap of markers.

parameter-space properties have been developed in order to efficiently cover large portions of the parameter space [20, 32, 33, 49–52, 61, 62, 79, 84, 86].

In this work, we have studied the performance of a general GPU-accelerated search, **fasttracks**, which we release as an open-source Python package [53]. We find that the simple brute-force implementation of short-coherence detection statistics using GPU-capable array language [94, 97, 98] provides a computational efficiency comparable to that of GPU-accelerated pipelines for similar detection statistics, such as [52, 91], at a lower code complexity. This promising result will be key to develop computationally-efficient methods to search for more realistic NS physics [36, 38, 40], as well as other, more exotic CW sources [8–19]. Similar strategies were used as part of the winning solutions in a recent Kaggle data analysis competition for CW signals [131].

Furthermore, we have explored the formulation of template-bank setup and post-processing algorithms. Notably, we have proposed an alternative to clustering algorithms based on preemptively splitting the parameter space into disjoint regions. This has the advantage of being simpler to implement and free from configuration choices such as parameter-spaces distance of clustering-specific parameters. Moreover, this procedure is easy to model from a statistical point of view. The feasibility of this approach has been successfully tested on a real-data application using data from the LVK’s third observing run. These results suggest alternative post-processing algorithms, such as [110, 111], may improve upon current clustering approaches in terms of computing cost and computational complexity.

Finally, we have generalized the sensitivity estimate

procedure presented in [54, 55, 119] to short-coherence detection statistics and to account for post-processing strategies such as the ones here presented. This will allow for a significant computing-cost reduction of all-sky sensitivity estimates and a better understanding of the optimal set up of real-data searches. We release this algorithm as part of the **cows3** [56, 57] open-source package.

The success of these simple ideas in the search for CW signals will become increasingly relevant for the search of long-duration GW signals such as those to come with next generation detectors [24–28].

## ACKNOWLEDGEMENTS

We thank Rafel Jaume, David Keitel, Andrew Miller, and the CW working group of the LIGO-Virgo-KAGRA Collaboration for comments on the manuscript. We also thank Frédéric Bastien, Michel Herrera Sanchez, Mahmoud Solimand, and Yu-Hang Tang for their support during the CINECA Open Hackathon 2023. This work was supported by the Universitat de les Illes Balears (UIB); the Spanish Agencia Estatal de Investigación grants PID2022-138626NB-I00, RED2022-134204-E, RED2022-134411-T, funded by MICIU/AEI/10.13039/501100011033, and ERDF/UE; the MICIU with funding from the European Union NextGenerationEU/PRTR (PRTR-C17.11); the Comunitat Autònoma de les Illes Balears through the Direcció General de Recerca, Innovació i Transformació Digital the Conselleria d’Economia, Hisenda i Innovació grant number SINCO 2022/18146 (HiTech-IAC3-BIO) co-financed by the European Union and FEDER Operational Program 2021-2027 of the Balearic Islands. RT is supported by ERC Starting Grant No. 945155–GWmining, Cariplo Foundation Grant No. 2021-0555, MUR PRIN Grant No. 2022-Z9X4XS, MUR Grant “Progetto Dipartimenti di Eccellenza 2023-2027” (BiCoQ), and the ICSC National Research Centre funded by NextGenerationEU. JRM is supported by the Spanish Ministerio de Ciencia, Innovación y Universidades (ref. FPU 22/01187). The authors are grateful for computing resources at Artemisa, funded by the European Union ERDF and Comunitat Valenciana as well as the technical support provided by the Instituto de Física Corpuscular, IFIC (CSIC-UV); MareNostrum5, as well as the technical support provided by Barcelona Supercomputing Center (RES-FI-2024-3-0013); the Digital Research Alliance of Canada (alliancecan.ca); and the LIGO Laboratory, which is supported by National Science Foundation Grants PHY-0757058 and PHY-0823459. This material is based upon work supported by NSF’s LIGO Laboratory which is a major facility fully funded by the National Science Foundation This research has made use of data or software obtained from the Gravitational Wave Open Science Center (gwosc.org), a service of the LIGO Scientific Collaboration, the Virgo Collaboration, and KAGRA. This material is based upon work supported by



NSF's LIGO Laboratory which is a major facility fully funded by the National Science Foundation, as well as the Science and Technology Facilities Council (STFC) of the United Kingdom, the Max-Planck-Society (MPS), and the State of Niedersachsen/Germany for support of the construction of Advanced LIGO and construction and operation of the GEO600 detector. Additional support for Advanced LIGO was provided by the Australian Research Council. Virgo is funded, through the European Gravitational Observatory (EGO), by the French Centre National de Recherche Scientifique (CNRS), the Italian Istituto Nazionale di Fisica Nucleare (INFN) and the Dutch Nikhef, with contributions by institutions from Belgium, Germany, Greece, Hungary, Ireland, Japan, Monaco, Poland, Portugal, Spain. KAGRA is supported by Ministry of Education, Culture, Sports, Science and Technology (MEXT), Japan Society for the Promotion of Science (JSPS) in Japan; National Research Foundation (NRF) and Ministry of Science and ICT (MSIT) in Korea; Academia Sinica (AS) and National Science and Technology Council (NSTC) in Taiwan. This document has been assigned document number LIGO-P2400425.

### Appendix A: Uniform coordinates for sources in circular binary systems

In this section we work out the uniform-density coordinates  $\xi$  for the case of sources in circular binary systems [Eq. (1)]. These choices are motivated by previous well-established approaches in the literature [33, 49, 67, 73, 82].

#### 1. Parameter-space resolution

We start by taking frequency resolution as

$$\delta f_0 = T_{\text{SFT}}^{-1}. \quad (\text{A1})$$

This is a conservative choice [33, 67, 132]. Frequency is inferred by essentially counting cycles; in that sense higher frequencies may be easier to determine, but the difference is small enough to be negligible for us for the sake of simplicity.

Similarly, the sky is highly anisotropic, as different Doppler modulations produce different resolutions. We take the minimal sky resolution to be our sky resolution, in a similar manner to [33]

$$\delta \text{sky} = (T_{\text{SFT}} v/c)^{-2} f_0^{-2}. \quad (\text{A2})$$

For binary orbital parameters, the general formulae derived following Eq. (26) tend to contain trigonometric expressions such as  $\sin(\Omega t + \phi_b)$  or  $\cos(\Omega t + \phi_b)$ . We distinguish two cases. First, the projected semimajor axis  $a_p$  and the binary orbital phase  $\phi_b$ :

$$\frac{\partial}{\partial a_p} f(t; \lambda) = f_0 \Omega \cos(\Omega t + \phi_b), \quad (\text{A3})$$

$$\frac{\partial}{\partial \phi_b} f(t; \lambda) = f_0 a_p \Omega^2 \sin(\Omega t + \phi_b). \quad (\text{A4})$$

To remove the time dependency, we conservatively set trigonometric expressions so that the smallest possible resolution is obtained:

$$\delta a_p = T_{\text{SFT}}^{-1} (f_0 \Omega)^{-1}, \quad (\text{A5})$$

$$\delta \phi_b = T_{\text{SFT}}^{-1} (f_0 a_p \Omega)^{-1}. \quad (\text{A6})$$

Second, the orbital frequency  $\Omega$ :

$$\frac{\partial}{\partial \Omega} f(t; \lambda) = f_0 a_p [\Omega(t + \phi_b) \sin(\Omega t + \phi_b) - \cos(\Omega t + \phi_b)]. \quad (\text{A7})$$

The sharpest possible resolution is obtained by maximising Eq. (A7). We assume to be working in a regime in which the orbital frequency is well resolved, i.e.  $\Omega T_{\text{obs}} \gg 1$ . In such case, the sinusoid term dominates and the narrowest resolution is obtained by setting it to 1:

$$\delta \Omega = (T_{\text{SFT}} T_{\text{obs}})^{-1} (f_0 a_p \Omega)^{-1}. \quad (\text{A8})$$

Note that these resolutions have the same functional dependency on  $\lambda$  as those obtained using the semicoherent metric in the short-segment limit by [63, 64] ( $T_{\text{SFT}} \ll 2\pi/\Omega$  in our notation).

#### 2. Coordinate transformation

The resulting local density of templates in the parameter space is

$$\varrho(\lambda) = k f_0^5 a_p^2 \Omega^3 \quad (\text{A9})$$

with  $k = T_{\text{SFT}}^6 T_{\text{obs}} (v/c)^2$ . Searches for this kind of signals are conducted all-sky, in narrow frequency bands, covering a region of the  $(a_p, \Omega)$  plane an the full range  $\phi_b \in [0, 2\pi)$ . The number of templates to place in said region according to our prescription is

$$\mathcal{N} = k \int_{f_{\text{min}}}^{f_{\text{max}}} df_0 f_0^5 \int_{S^2} d\text{sky} \int_{a_p^{\text{min}}}^{a_p^{\text{max}}} da_p a_p^2 \int_{\Omega^{\text{min}}}^{\Omega^{\text{max}}} d\Omega \Omega^3 \int_0^{2\pi} d\phi_b. \quad (\text{A10})$$

Two minor details are to be mentioned. First,  $d\text{sky}$  is a solid angle integral. We conduct our search using equatorial coordinates, which means the corresponding parameters will be the right ascension  $\alpha$  and the *sine* of the declination  $\sin \delta$ . Second, this expression explains the usage of  $\phi_b$  instead of  $t_{\text{asc}} = \phi_b/\Omega$ , as otherwise the limits in the  $dt_{\text{asc}}$  would depend on  $\Omega$  and the integral would not be separable.

Since the integral in Eq. (A10) is separable, we use of Eq. (32) to derive the corresponding uniform coordinates:

$$\begin{aligned}
 \xi[0] &= \frac{k^{1/6}}{6} f_0^6 \\
 \xi[1] &= k^{1/6} \alpha \\
 \xi[2] &= k^{1/6} \sin \delta \\
 \xi[3] &= \frac{k^{1/6}}{3} a_p^3 \\
 \xi[4] &= \frac{k^{1/6}}{4} \Omega^4 \\
 \xi[5] &= k^{1/6} \phi_b
 \end{aligned} \tag{A11}$$

Note that overall constants can be freely distributed

across all coordinates insofar  $d\xi = d\lambda\varrho(\lambda)$ .

The setup of a template bank is now trivial. First, we transform the parameter-space limits from  $\lambda$  to  $\xi$  using Eq. (A11). This results in a hyperbox bounded by

$$\xi_{\min} = \{\xi(\lambda[k]_{\min}), k = 0, \dots, 5\}, \tag{A12}$$

$$\xi_{\max} = \{\xi(\lambda[k]_{\max}), k = 0, \dots, 5\}. \tag{A13}$$

Now, to set up a random template bank, we draw random uniform arrays within the computed bounds  $\xi_i \sim \mathcal{U}(\xi_{\min}, \xi_{\max})$  and map them back to the  $\lambda$  space using the inverse transformation of Eq. (A11)  $\lambda_i = \lambda(\xi_i)$ .

- 
- [1] K. Riles, Searches for continuous-wave gravitational radiation, *Living Rev. Rel.* **26**, 3 (2023), [arXiv:2206.06447 \[astro-ph.HE\]](#).
- [2] J. Aasi *et al.* (LIGO Scientific), Advanced LIGO, *Class. Quant. Grav.* **32**, 074001 (2015), [arXiv:1411.4547 \[gr-qc\]](#).
- [3] F. Acernese *et al.* (VIRGO), Advanced Virgo: a second-generation interferometric gravitational wave detector, *Class. Quant. Grav.* **32**, 024001 (2015), [arXiv:1408.3978 \[gr-qc\]](#).
- [4] T. Akutsu *et al.* (KAGRA), KAGRA: 2.5 Generation Interferometric Gravitational Wave Detector, *Nature Astron.* **3**, 35 (2019), [arXiv:1811.08079 \[gr-qc\]](#).
- [5] M. Sieniawska and M. Bejger, Continuous gravitational waves from neutron stars: current status and prospects, *Universe* **5**, 217 (2019), [arXiv:1909.12600 \[astro-ph.HE\]](#).
- [6] O. J. Piccinni, Status and Perspectives of Continuous Gravitational Wave Searches, *Galaxies* **10**, 72 (2022), [arXiv:2202.01088 \[gr-qc\]](#).
- [7] B. Haskell and M. Bejger, Astrophysics with continuous gravitational waves, *Nature Astronomy* **7**, 1160 (2023).
- [8] M. Isi, L. Sun, R. Brito, and A. Melatos, Directed searches for gravitational waves from ultralight bosons, *Phys. Rev. D* **99**, 084042 (2019), [Erratum: *Phys. Rev. D* **102**, 049901 (2020)], [arXiv:1810.03812 \[gr-qc\]](#).
- [9] L. Sun, R. Brito, and M. Isi, Search for ultralight bosons in Cygnus X-1 with Advanced LIGO, *Phys. Rev. D* **101**, 063020 (2020), [Erratum: *Phys. Rev. D* **102**, 089902 (2020)], [arXiv:1909.11267 \[gr-qc\]](#).
- [10] C. Palomba *et al.*, Direct constraints on ultralight boson mass from searches for continuous gravitational waves, *Phys. Rev. Lett.* **123**, 171101 (2019), [arXiv:1909.08854 \[astro-ph.HE\]](#).
- [11] S. J. Zhu, M. Baryakhtar, M. A. Papa, D. Tsuna, N. Kawanaka, and H.-B. Eggenstein, Characterizing the continuous gravitational-wave signal from boson clouds around Galactic isolated black holes, *Phys. Rev. D* **102**, 063020 (2020), [arXiv:2003.03359 \[gr-qc\]](#).
- [12] D. Jones, L. Sun, N. Siemonsen, W. E. East, S. M. Scott, and K. Wette, Methods and prospects for gravitational-wave searches targeting ultralight vector-boson clouds around known black holes, *Phys. Rev. D* **108**, 064001 (2023), [arXiv:2305.00401 \[gr-qc\]](#).
- [13] A. L. Miller, F. Badaracco, and C. Palomba (LIGO Scientific, Virgo, KAGRA), Distinguishing between dark-matter interactions with gravitational-wave detectors, *Phys. Rev. D* **105**, 103035 (2022), [arXiv:2204.03814 \[astro-ph.IM\]](#).
- [14] A. L. Miller and L. Mendes, First search for ultralight dark matter with a space-based gravitational-wave antenna: LISA Pathfinder, *Phys. Rev. D* **107**, 063015 (2023), [arXiv:2301.08736 \[gr-qc\]](#).
- [15] A. G. Abac *et al.* (KAGRA, LIGO Scientific, VIRGO), Ultralight vector dark matter search using data from the KAGRA O3GK run, *Phys. Rev. D* **110**, 042001 (2024), [arXiv:2403.03004 \[astro-ph.CO\]](#).
- [16] S. Bhattacharya, A. L. Miller, and A. Ray, Continuous gravitational waves: A new window to look for heavy nonannihilating dark matter, *Phys. Rev. D* **110**, 043006 (2024), [arXiv:2403.13886 \[hep-ph\]](#).
- [17] H.-K. Guo and A. Miller, Searching for Mini Extreme Mass Ratio Inspirals with Gravitational-Wave Detectors, *arXiv e-prints* (2022), [arXiv:2205.10359 \[astro-ph.IM\]](#).
- [18] A. L. Miller, Prospects for detecting asteroid-mass primordial black holes in extreme-mass-ratio inspirals with continuous gravitational waves, *arXiv e-prints* (2024), [arXiv:2410.01348 \[gr-qc\]](#).
- [19] A. L. Miller, N. Aggarwal, S. Clesse, F. De Lillo, S. Sachdev, P. Astone, C. Palomba, O. J. Piccinni, and L. Pierini, Gravitational Wave Constraints on Planetary-Mass Primordial Black Holes Using LIGO O3a Data, *Phys. Rev. Lett.* **133**, 111401 (2024), [arXiv:2402.19468 \[gr-qc\]](#).
- [20] P. Jaranowski, A. Krolak, and B. F. Schutz, Data analysis of gravitational - wave signals from spinning neutron stars. 1. The Signal and its detection, *Phys. Rev. D* **58**, 063001 (1998), [arXiv:gr-qc/9804014](#).
- [21] C. Cutler and B. F. Schutz, The Generalized F-statistic: Multiple detectors and multiple GW pulsars, *Phys. Rev. D* **72**, 063006 (2005), [arXiv:gr-qc/0504011](#).
- [22] P. R. Brady and T. Creighton, Searching for periodic sources with LIGO. 2. Hierarchical searches, *Phys. Rev. D* **61**, 082001 (2000), [arXiv:gr-qc/9812014](#).
- [23] K. Wette, Lattice template placement for coherent all-sky searches for gravitational-wave pulsars, *Phys. Rev. D* **90**, 122010 (2014), [arXiv:1410.6882 \[gr-qc\]](#).
- [24] M. Maggiore *et al.*, Science Case for the Einstein

- Telescope, *JCAP* **03**, 050, [arXiv:1912.02622 \[astro-ph.CO\]](#).
- [25] D. Reitze *et al.*, Cosmic Explorer: The U.S. Contribution to Gravitational-Wave Astronomy beyond LIGO, *Bull. Am. Astron. Soc.* **51**, 035 (2019), [arXiv:1907.04833 \[astro-ph.IM\]](#).
- [26] P. Amaro-Seoane *et al.*, Laser Interferometer Space Antenna, [arXiv e-prints](#), [arXiv:1702.00786 \(2017\)](#), [arXiv:1702.00786 \[astro-ph.IM\]](#).
- [27] W.-R. Hu and Y.-L. Wu, The Taiji Program in Space for gravitational wave physics and the nature of gravity, *Natl. Sci. Rev.* **4**, 685 (2017).
- [28] E.-K. Li *et al.*, Gravitational Wave Astronomy With TianQin, [arXiv e-prints](#) (2024), [arXiv:2409.19665 \[astro-ph.GA\]](#).
- [29] R. Abbott *et al.* (KAGRA, VIRGO, LIGO Scientific), GWTC-3: Compact Binary Coalescences Observed by LIGO and Virgo during the Second Part of the Third Observing Run, *Phys. Rev. X* **13**, 041039 (2023), [arXiv:2111.03606 \[gr-qc\]](#).
- [30] D. Wadekar, J. Roulet, T. Venumadhav, A. K. Mehta, B. Zackay, J. Mushkin, S. Olsen, and M. Zaldarriaga, New black hole mergers in the LIGO-Virgo O3 data from a gravitational wave search including higher-order harmonics, [arXiv e-print](#) (2023), [arXiv:2312.06631 \[gr-qc\]](#).
- [31] B. P. Abbott *et al.* (LIGO Scientific, Virgo), The basic physics of the binary black hole merger GW150914, *Annalen Phys.* **529**, 1600209 (2017), [arXiv:1608.01940 \[gr-qc\]](#).
- [32] P. Astone, K. M. Borkowski, P. Jaranowski, and A. Krolak, Data analysis of gravitational wave signals from spinning neutron stars. 4. An All sky search, *Phys. Rev. D* **65**, 042003 (2002), [arXiv:gr-qc/0012108](#).
- [33] B. Krishnan, A. M. Sintes, M. A. Papa, B. F. Schutz, S. Frasca, and C. Palomba, The Hough transform search for continuous gravitational waves, *Phys. Rev. D* **70**, 082001 (2004), [arXiv:gr-qc/0407001](#).
- [34] K. Wette, Searches for continuous gravitational waves from neutron stars: A twenty-year retrospective, *Astropart. Phys.* **153**, 102880 (2023), [arXiv:2305.07106 \[gr-qc\]](#).
- [35] R. Tenorio, D. Keitel, and A. M. Sintes, Search Methods for Continuous Gravitational-Wave Signals from Unknown Sources in the Advanced-Detector Era, *Universe* **7**, 474 (2021), [arXiv:2111.12575 \[gr-qc\]](#).
- [36] G. Ashton, R. Prix, and D. I. Jones, Statistical characterization of pulsar glitches and their potential impact on searches for continuous gravitational waves, *Phys. Rev. D* **96**, 063004 (2017), [arXiv:1704.00742 \[gr-qc\]](#).
- [37] G. Ashton, R. Prix, and D. I. Jones, A semicoherent glitch-robust continuous-gravitational-wave search method, *Phys. Rev. D* **98**, 063011 (2018), [arXiv:1805.03314 \[gr-qc\]](#).
- [38] A. Mukherjee, C. Messenger, and K. Riles, Accretion-induced spin-wandering effects on the neutron star in Scorpius X-1: Implications for continuous gravitational wave searches, *Phys. Rev. D* **97**, 043016 (2018), [arXiv:1710.06185 \[gr-qc\]](#).
- [39] P. B. Covas, Effects of proper motion of neutron stars on continuous gravitational-wave searches, *Mon. Not. Roy. Astron. Soc.* **500**, 5167 (2020), [arXiv:2008.00983 \[astro-ph.IM\]](#).
- [40] M. Sieniawska, D. I. Jones, and A. L. Miller, Measuring neutron star distances and properties with gravitational-wave parallax, *Mon. Not. Roy. Astron. Soc.* **521**, 1924 (2023), [arXiv:2212.07506 \[astro-ph.HE\]](#).
- [41] R. Prix, S. Giampanis, and C. Messenger, Search method for long-duration gravitational-wave transients from neutron stars, *Phys. Rev. D* **84**, 023007 (2011), [arXiv:1104.1704 \[gr-qc\]](#).
- [42] P. D. Lasky, N. Sarin, and L. Sammut, Long-duration waveform models for millisecond magnetars born in binary neutron star mergers, <https://dcc.ligo.org/LIGO-T1700408/public> (2017), Tech. Rep. LIGO-T1700408.
- [43] N. Sarin, P. D. Lasky, L. Sammut, and G. Ashton, X-ray guided gravitational-wave search for binary neutron star merger remnants, *Phys. Rev. D* **98**, 043011 (2018), [arXiv:1805.01481 \[astro-ph.HE\]](#).
- [44] N. Siemonsen, T. May, and W. E. East, Modeling the black hole superradiance gravitational waveform, *Phys. Rev. D* **107**, 104003 (2023), [arXiv:2211.03845 \[gr-qc\]](#).
- [45] A. L. Miller, N. Singh, and C. Palomba, Enabling multimessenger astronomy with continuous gravitational waves: Early warning and sky localization of binary neutron stars in the Einstein Telescope, *Phys. Rev. D* **109**, 043021 (2024), [arXiv:2309.15808 \[astro-ph.IM\]](#).
- [46] B. Allen, E. Goetz, D. Keitel, M. Landry, G. Mendell, R. Prix, K. Riles, and K. Wette, SFT Data Format Version 2–3 Specification, <https://dcc.ligo.org/LIGO-T040164> (2022), T040164.
- [47] P. Astone, S. Frasca, and C. Palomba, The short FFT database and the peak map for the hierarchical search of periodic sources, *Class. Quant. Grav.* **22**, S1197 (2005).
- [48] O. J. Piccinni, P. Astone, S. D’Antonio, S. Frasca, G. Intini, P. Leaci, S. Mastrogiovanni, A. Miller, C. Palomba, and A. Singhal, A new data analysis framework for the search of continuous gravitational wave signals, *Class. Quant. Grav.* **36**, 015008 (2019), [arXiv:1811.04730 \[gr-qc\]](#).
- [49] P. Astone, A. Colla, S. D’Antonio, S. Frasca, and C. Palomba, Method for all-sky searches of continuous gravitational wave signals using the frequency-Hough transform, *Phys. Rev. D* **90**, 042002 (2014), [arXiv:1407.8333 \[astro-ph.IM\]](#).
- [50] A. Miller *et al.*, Method to search for long duration gravitational wave transients from isolated neutron stars using the generalized frequency-Hough transform, *Phys. Rev. D* **98**, 102004 (2018), [arXiv:1810.09784 \[astro-ph.IM\]](#).
- [51] M. Oliver, D. Keitel, and A. M. Sintes, Adaptive transient Hough method for long-duration gravitational wave transients, *Phys. Rev. D* **99**, 104067 (2019), [arXiv:1901.01820 \[gr-qc\]](#).
- [52] P. B. Covas and A. M. Sintes, New method to search for continuous gravitational waves from unknown neutron stars in binary systems, *Phys. Rev. D* **99**, 124019 (2019), [arXiv:1904.04873 \[astro-ph.IM\]](#).
- [53] R. Tenorio and J.-R. M erou, *FastTracks*, <https://github.com/Rodrigo-Tenorio/fasttracks> (2024).
- [54] K. Wette, Estimating the sensitivity of wide-parameter-space searches for gravitational-wave pulsars, *Phys. Rev. D* **85**, 042003 (2012), [arXiv:1111.5650 \[gr-qc\]](#).
- [55] C. Dreissigacker, R. Prix, and K. Wette, Fast and Accurate Sensitivity Estimation for Continuous-Gravitational-Wave Searches, *Phys. Rev. D* **98**, 084058 (2018), [arXiv:1808.02459 \[gr-qc\]](#).

- [56] L. Mirasola and R. Tenorio, Towards a computationally-efficient follow-up pipeline for blind continuous gravitational-wave searches, arXiv e-prints (2024), [arXiv:2405.18934 \[gr-qc\]](https://arxiv.org/abs/2405.18934).
- [57] R. Tenorio and L. Mirasola, cows3: continuous-wave search sensitivity simulator, <https://github.com/Rodrigo-Tenorio/continuous-wave-search-sensitivity-simulator> (2024), v0.1.0.
- [58] R. Abbott *et al.* (KAGRA, VIRGO, LIGO Scientific), Open Data from the Third Observing Run of LIGO, Virgo, KAGRA, and GEO, *Astrophys. J. Suppl.* **267**, 29 (2023), [arXiv:2302.03676 \[gr-qc\]](https://arxiv.org/abs/2302.03676).
- [59] C. Cutler, I. Gholami, and B. Krishnan, Improved stack-slide searches for gravitational-wave pulsars, *Phys. Rev. D* **72**, 042004 (2005), [arXiv:gr-qc/0505082](https://arxiv.org/abs/gr-qc/0505082).
- [60] R. Prix and M. Shaltev, Search for Continuous Gravitational Waves: Optimal StackSlide method at fixed computing cost, *Phys. Rev. D* **85**, 084010 (2012), [arXiv:1201.4321 \[gr-qc\]](https://arxiv.org/abs/1201.4321).
- [61] V. Dergachev, Description of PowerFlux algorithms and implementation, <https://dcc.ligo.org/LIGO-T050186/public> (2006).
- [62] V. Dergachev, Description of PowerFlux 2 algorithms and implementation, <https://dcc.ligo.org/LIGO-T1000272/public> (2011).
- [63] C. Messenger, A semi-coherent search strategy for known continuous wave sources in binary systems, *Phys. Rev. D* **84**, 083003 (2011), [arXiv:1109.0501 \[gr-qc\]](https://arxiv.org/abs/1109.0501).
- [64] P. Leaci and R. Prix, Directed searches for continuous gravitational waves from binary systems: parameter-space metrics and optimal Scorpius X-1 sensitivity, *Phys. Rev. D* **91**, 102003 (2015), [arXiv:1502.00914 \[gr-qc\]](https://arxiv.org/abs/1502.00914).
- [65] C. Palomba, P. Astone, and S. Frasca, Adaptive hough transform for the search of periodic sources, *Class. Quant. Grav.* **22**, S1255 (2005).
- [66] B. Abbott *et al.* (LIGO Scientific), All-sky search for periodic gravitational waves in LIGO S4 data, *Phys. Rev. D* **77**, 022001 (2008), [Erratum: *Phys.Rev.D* 80, 129904 (2009)], [arXiv:0708.3818 \[gr-qc\]](https://arxiv.org/abs/0708.3818).
- [67] B. Allen, M. A. Papa, and B. F. Schutz, Optimal strategies for sinusoidal signal detection, *Phys. Rev. D* **66**, 102003 (2002), [arXiv:gr-qc/0206032](https://arxiv.org/abs/gr-qc/0206032).
- [68] R. Prix,  $\mathcal{F}$ -statistic bias due to noise-estimator, <https://dcc.ligo.org/LIGO-T1100551/public> (2011).
- [69] C. Rover, R. Meyer, and N. Christensen, Modelling coloured residual noise in gravitational-wave signal processing, *Class. Quant. Grav.* **28**, 015010 (2011), [arXiv:0804.3853 \[stat.ME\]](https://arxiv.org/abs/0804.3853).
- [70] C. Rover, A Student-t based filter for robust signal detection, *Phys. Rev. D* **84**, 122004 (2011), [arXiv:1109.0442 \[physics.data-an\]](https://arxiv.org/abs/1109.0442).
- [71] A. Sasli, N. Karnesis, and N. Stergioulas, Heavy-tailed likelihoods for robustness against data outliers: Applications to the analysis of gravitational wave data, *Phys. Rev. D* **108**, 103005 (2023), [arXiv:2305.04709 \[gr-qc\]](https://arxiv.org/abs/2305.04709).
- [72] LIGO Scientific Collaboration, Virgo Collaboration, and KAGRA Collaboration, *LVK Algorithm Library - LALSuite*, Free software (GPL) (2018).
- [73] R. Prix, Search for continuous gravitational waves: Metric of the multi-detector  $F$ -statistic, *Phys. Rev. D* **75**, 023004 (2007), [Erratum: *Phys.Rev.D* 75, 069901 (2007)], [arXiv:gr-qc/0606088](https://arxiv.org/abs/gr-qc/0606088).
- [74] R. Prix, Template-based searches for gravitational waves: Efficient lattice covering of flat parameter spaces, *Class. Quant. Grav.* **24**, S481 (2007), [arXiv:0707.0428 \[gr-qc\]](https://arxiv.org/abs/0707.0428).
- [75] B. Allen, Optimal template banks, *Phys. Rev. D* **104**, 042005 (2021), [arXiv:2102.11254 \[astro-ph.IM\]](https://arxiv.org/abs/2102.11254).
- [76] P. R. Williams and B. F. Schutz, An Efficient matched filtering algorithm for the detection of continuous gravitational wave signals, *AIP Conf. Proc.* **523**, 473 (2000), [arXiv:gr-qc/9912029](https://arxiv.org/abs/gr-qc/9912029).
- [77] H. J. Pletsch and B. Allen, Exploiting global correlations to detect continuous gravitational waves, *Phys. Rev. Lett.* **103**, 181102 (2009), [arXiv:0906.0023 \[gr-qc\]](https://arxiv.org/abs/0906.0023).
- [78] P. Patel, X. Siemens, R. Dupuis, and J. Betzwieser, Implementation of barycentric resampling for continuous wave searches in gravitational wave data, *Phys. Rev. D* **81**, 084032 (2010), [arXiv:0912.4255 \[gr-qc\]](https://arxiv.org/abs/0912.4255).
- [79] V. Dergachev, On blind searches for noise dominated signals: a loosely coherent approach, *Class. Quant. Grav.* **27**, 205017 (2010), [arXiv:1003.2178 \[gr-qc\]](https://arxiv.org/abs/1003.2178).
- [80] V. Dergachev, Loosely coherent searches for sets of well-modeled signals, *Phys. Rev. D* **85**, 062003 (2012), [arXiv:1110.3297 \[gr-qc\]](https://arxiv.org/abs/1110.3297).
- [81] G. D. Meadors, B. Krishnan, M. A. Papa, J. T. Whelan, and Y. Zhang, Resampling to accelerate cross-correlation searches for continuous gravitational waves from binary systems, *Phys. Rev. D* **97**, 044017 (2018), [arXiv:1712.06515 \[astro-ph.IM\]](https://arxiv.org/abs/1712.06515).
- [82] K. Wette, S. Walsh, R. Prix, and M. A. Papa, Implementing a semicoherent search for continuous gravitational waves using optimally-constructed template banks, *Phys. Rev. D* **97**, 123016 (2018), [arXiv:1804.03392 \[astro-ph.IM\]](https://arxiv.org/abs/1804.03392).
- [83] V. Dergachev, Loosely coherent searches for medium scale coherence lengths, arXiv e-prints (2018), [arXiv:1807.02351 \[astro-ph.IM\]](https://arxiv.org/abs/1807.02351).
- [84] V. Dergachev and M. A. Papa, Sensitivity improvements in the search for periodic gravitational waves using O1 LIGO data, *Phys. Rev. Lett.* **123**, 101101 (2019), [arXiv:1902.05530 \[gr-qc\]](https://arxiv.org/abs/1902.05530).
- [85] R. Prix, The  $F$ -statistic and its implementation in ComputeFStatistic\_v2, <https://dcc.ligo.org/LIGO-T0900149/public> (2019).
- [86] P. B. Covas and R. Prix, Improved all-sky search method for continuous gravitational waves from unknown neutron stars in binary systems, *Phys. Rev. D* **106**, 084035 (2022), [arXiv:2208.01543 \[gr-qc\]](https://arxiv.org/abs/2208.01543).
- [87] M. Andrés-Carcasona, O. J. Piccinni, M. Martínez, and L.-M. Mir, BSD-COBI: New search pipeline to target inspiraling light dark compact objects., *PoS EPS-HEP2023*, 067 (2024).
- [88] A. L. Miller, N. Aggarwal, S. Clesse, F. De Lillo, S. Sachdev, P. Astone, C. Palomba, O. J. Piccinni, and L. Pierini, Method to search for inspiraling planetary-mass ultracompact binaries using the generalized frequency-Hough transform in LIGO O3a data, *Phys. Rev. D* **110**, 082004 (2024), [arXiv:2407.17052 \[astro-ph.IM\]](https://arxiv.org/abs/2407.17052).
- [89] NVIDIA, P. Vingelmann, and F. H. Fitzek, Cuda, release: 10.2.89, <https://developer.nvidia.com/cuda-toolkit> (2020).
- [90] D. Keitel and G. Ashton, Faster search for long gravitational-wave transients: GPU implementation



- of the transient  $\mathcal{F}$ -statistic, *Class. Quant. Grav.* **35**, 205003 (2018), [arXiv:1805.05652 \[astro-ph.IM\]](#).
- [91] I. L. Rosa, P. Astone, S. D’Antonio, S. Frasca, P. Leaci, A. L. Miller, C. Palomba, O. J. Piccinni, L. Pierini, and T. Regimbau, Continuous Gravitational-Wave Data Analysis with General Purpose Computing on Graphic Processing Units, *Universe* **7**, 218 (2021).
- [92] L. Dunn, P. Clearwater, A. Melatos, and K. Wette, Graphics processing unit implementation of the  $\mathcal{F}$ -statistic for continuous gravitational wave searches, *Class. Quant. Grav.* **39**, 045003 (2022), [arXiv:2201.00451 \[gr-qc\]](#).
- [93] M. Bejger *et al.*, `polgraw-allsky`, <https://github.com/mbejger/polgraw-allsky>.
- [94] R. Frostig, M. Johnson, and C. Leary, Compiling machine learning programs via high-level tracing (2018).
- [95] J. Bradbury, R. Frostig, P. Hawkins, M. J. Johnson, C. Leary, D. Maclaurin, G. Necula, A. Paszke, J. VanderPlas, S. Wanderman-Milne, and Q. Zhang, JAX: composable transformations of Python+NumPy programs, <http://github.com/google/jax> (2018).
- [96] C. R. Harris, K. J. Millman, S. J. van der Walt, R. Gommers, P. Virtanen, D. Cournapeau, E. Wieser, J. Taylor, S. Berg, N. J. Smith, R. Kern, M. Picus, S. Hoyer, M. H. van Kerkwijk, M. Brett, A. Haldane, J. F. del Río, M. Wiebe, P. Peterson, P. Gérard-Marchant, K. Sheppard, T. Reddy, W. Weckesser, H. Abbasi, C. Gohlke, and T. E. Oliphant, Array programming with NumPy, *Nature* **585**, 357 (2020).
- [97] R. Okuta, Y. Unno, D. Nishino, S. Hido, and C. Loomis, Cupy: A numpy-compatible library for nvidia gpu calculations, in *Proceedings of Workshop on Machine Learning Systems (LearningSys) in The Thirty-first Annual Conference on Neural Information Processing Systems (NIPS)* (2017).
- [98] A. Paszke, S. Gross, F. Massa, A. Lerer, J. Bradbury, G. Chanan, T. Killeen, Z. Lin, N. Gimelshein, L. Antiga, A. Desmaison, A. Köpf, E. Yang, Z. DeVito, M. Raison, A. Tejani, S. Chilamkurthy, B. Steiner, L. Fang, J. Bai, and S. Chintala, PyTorch: An Imperative Style, High-Performance Deep Learning Library, [arXiv e-prints](#), [arXiv:1912.01703 \(2019\)](#), [arXiv:1912.01703 \[cs.LG\]](#).
- [99] R. Prix and B. Krishnan, Targeted search for continuous gravitational waves: Bayesian versus maximum-likelihood statistics, *Class. Quant. Grav.* **26**, 204013 (2009), [arXiv:0907.2569 \[gr-qc\]](#).
- [100] K. J. Wagner, J. T. Whelan, J. K. Wofford, and K. Wette, Template lattices for a cross-correlation search for gravitational waves from Scorpius X-1, *Class. Quant. Grav.* **39**, 075013 (2022), [arXiv:2106.16142 \[gr-qc\]](#).
- [101] H. J. Pletsch, Parameter-space metric of semicoherent searches for continuous gravitational waves, *Phys. Rev. D* **82**, 042002 (2010), [arXiv:1005.0395 \[gr-qc\]](#).
- [102] D. Keitel, G. Woan, M. Pitkin, C. Schumacher, B. Pearlstone, K. Riles, A. G. Lyne, J. Palfreyman, B. Stappers, and P. Weltevrede, First search for long-duration transient gravitational waves after glitches in the Vela and Crab pulsars, *Phys. Rev. D* **100**, 064058 (2019), [arXiv:1907.04717 \[gr-qc\]](#).
- [103] R. Tenorio, L. M. Modafferi, D. Keitel, and A. M. Sintes, Empirically estimating the distribution of the loudest candidate from a gravitational-wave search, *Phys. Rev. D* **105**, 044029 (2022), [arXiv:2111.12032 \[gr-qc\]](#).
- [104] R. Abbott *et al.* (LIGO Scientific, KAGRA, VIRGO), Narrowband Searches for Continuous and Long-duration Transient Gravitational Waves from Known Pulsars in the LIGO-Virgo Third Observing Run, *Astrophys. J.* **932**, 133 (2022), [arXiv:2112.10990 \[gr-qc\]](#).
- [105] K. Wette, L. Dunn, P. Clearwater, and A. Melatos, Deep exploration for continuous gravitational waves at 171–172 Hz in LIGO second observing run data, *Phys. Rev. D* **103**, 083020 (2021), [arXiv:2103.12976 \[gr-qc\]](#).
- [106] P. B. Covas *et al.*, Identification and mitigation of narrow spectral artifacts that degrade searches for persistent gravitational waves in the first two observing runs of Advanced LIGO, *Phys. Rev. D* **97**, 082002 (2018), [arXiv:1801.07204 \[astro-ph.IM\]](#).
- [107] A. Singh, M. A. Papa, H.-B. Eggenstein, and S. Walsh, Adaptive clustering procedure for continuous gravitational wave searches, *Phys. Rev. D* **96**, 082003 (2017), [arXiv:1707.02676 \[gr-qc\]](#).
- [108] F. Morawski, M. Bejger, and P. Ciecielag, Convolutional neural network classifier for the output of the time-domain  $\mathcal{F}$ -statistic all-sky search for continuous gravitational waves, *Machine Learning: Science and Technology* **1**, 025016 (2020).
- [109] R. Tenorio, D. Keitel, and A. M. Sintes, Time-frequency track distance for comparing continuous gravitational wave signals, *Phys. Rev. D* **103**, 064053 (2021), [arXiv:2012.05752 \[gr-qc\]](#).
- [110] B. Beheshtipour and M. A. Papa, Deep learning for clustering of continuous gravitational wave candidates, *Phys. Rev. D* **101**, 064009 (2020), [arXiv:2001.03116 \[gr-qc\]](#).
- [111] B. Beheshtipour and M. A. Papa, Deep learning for clustering of continuous gravitational wave candidates II: identification of low-SNR candidates, *Phys. Rev. D* **103**, 064027 (2021), [arXiv:2012.04381 \[gr-qc\]](#).
- [112] B. Steltner, T. Menne, M. A. Papa, and H.-B. Eggenstein, Density-clustering of continuous gravitational wave candidates from large surveys, *Phys. Rev. D* **106**, 104063 (2022), [arXiv:2207.14286 \[gr-qc\]](#).
- [113] K. Wette and R. Prix, Flat parameter-space metric for all-sky searches for gravitational-wave pulsars, *Phys. Rev. D* **88**, 123005 (2013), [arXiv:1310.5587 \[gr-qc\]](#).
- [114] K. Wette, Empirically extending the range of validity of parameter-space metrics for all-sky searches for gravitational-wave pulsars, *Phys. Rev. D* **94**, 122002 (2016), [arXiv:1607.00241 \[gr-qc\]](#).
- [115] C. Messenger, R. Prix, and M. A. Papa, Random template banks and relaxed lattice coverings, *Phys. Rev. D* **79**, 104017 (2009), [arXiv:0809.5223 \[gr-qc\]](#).
- [116] A. Coogan, T. D. P. Edwards, H. S. Chia, R. N. George, K. Freese, C. Messick, C. N. Setzer, C. Weniger, and A. Zimmerman, Efficient gravitational wave template bank generation with differentiable waveforms, *Phys. Rev. D* **106**, 122001 (2022), [arXiv:2202.09380 \[astro-ph.IM\]](#).
- [117] B. Allen, Performance of random template banks, *Phys. Rev. D* **105**, 102003 (2022), [arXiv:2203.02759 \[gr-qc\]](#).
- [118] B. Behnke, M. A. Papa, and R. Prix, Postprocessing methods used in the search for continuous gravitational-wave signals from the Galactic Center, *Phys. Rev. D* **91**, 064007 (2015), [arXiv:1410.5997 \[gr-qc\]](#).
- [119] K. Wette, R. Prix, D. Keitel, M. Pitkin, C. Dreissigacker, J. T. Whelan, and P. Leaci, OctApps: a library of Octave functions for continuous gravitational-wave data analysis, *Journal of Open Source Software* **3**, 707 (2018).

- [120] A. C. Searle, Monte-Carlo and Bayesian techniques in gravitational wave burst data analysis, in *12th Gravitational Wave Data Analysis Workshop* (2008) [arXiv:0804.1161 \[gr-qc\]](https://arxiv.org/abs/0804.1161).
- [121] E. T. Jaynes, *Probability theory: The logic of science*, edited by Bretthorst, G. L. (Cambridge University Press, Cambridge, 2003).
- [122] R. Prix, Analytic weak-signal approximation of the Bayes factor for continuous gravitational waves, arXiv e-prints (2024), [arXiv:2409.13069 \[gr-qc\]](https://arxiv.org/abs/2409.13069).
- [123] D. Keitel, R. Prix, M. A. Papa, P. Leaci, and M. Siddiqi, Search for continuous gravitational waves: Improving robustness versus instrumental artifacts, *Phys. Rev. D* **89**, 064023 (2014), [arXiv:1311.5738 \[gr-qc\]](https://arxiv.org/abs/1311.5738).
- [124] D. Keitel, Robust semicoherent searches for continuous gravitational waves with noise and signal models including hours to days long transients, *Phys. Rev. D* **93**, 084024 (2016), [arXiv:1509.02398 \[gr-qc\]](https://arxiv.org/abs/1509.02398).
- [125] P. B. Covas and R. Prix, Improved short-segment detection statistic for continuous gravitational waves, *Phys. Rev. D* **105**, 124007 (2022), [arXiv:2203.08723 \[gr-qc\]](https://arxiv.org/abs/2203.08723).
- [126] R. Abbott *et al.* (LIGO Scientific, Virgo, VIRGO), All-sky search in early O3 LIGO data for continuous gravitational-wave signals from unknown neutron stars in binary systems, *Phys. Rev. D* **103**, 064017 (2021), [Erratum: *Phys.Rev.D* 108, 069901 (2023)], [arXiv:2012.12128 \[gr-qc\]](https://arxiv.org/abs/2012.12128).
- [127] R. Tenorio, D. Keitel, and A. M. Sintes, Application of a hierarchical MCMC follow-up to Advanced LIGO continuous gravitational-wave candidates, *Phys. Rev. D* **104**, 084012 (2021), [arXiv:2105.13860 \[gr-qc\]](https://arxiv.org/abs/2105.13860).
- [128] P. B. Covas, R. Prix, and J. Martins, New framework to follow up candidates from continuous gravitational-wave searches, *Phys. Rev. D* **110**, 024053 (2024), [arXiv:2404.18608 \[gr-qc\]](https://arxiv.org/abs/2404.18608).
- [129] P. B. Covas, *Searching for continuous gravitational waves with Advanced LIGO*, Ph.D. thesis, University of the Balearic Islands (2020).
- [130] B. Krishnnan and A. M. Sintes, Hough search with improved sensitivity, <https://dcc.ligo.org/LIGO-T070124/public> (2007).
- [131] Tenorio, Rodrigo and Williams, Michael J., and Bayley, Joseph and Messenger, Chris and others, in prep., <https://dcc.ligo.org/LIGO-P2200295> (2024).
- [132] L. G. Bretthorst, *Bayesian Spectrum Analysis and Parameter Estimations* (Springer New York, NY, 1988).